*Revised Manuscript with No changes marked
Click here to download Revised Manuscript with No changes marked: Manuscript no changes marked.docx

Role of magma mixing in the pre-eruptive dynamics of the Aeolian Islands volcanoes (Southern Tyrrhenian Sea, Italy)

Stefano Rossi[1*], Maurizio Petrelli[1,2], Daniele Morgavi[1], Francesco P. Vetere[1], Renat R. Almeev[3], Rebecca L. Astbury[1], Diego Perugini[1]

[1] *Department of Physics and Geology, University of Perugia, Piazza Università 1, 06100 Perugia, Italy*

[2] *Istituto Nazionale di Fisica Nucleare, Sezione di Perugia, Via A. Pascoli, 06123, Perugia, Italy*

[3] *Institüt für Mineralogie, Leibniz Universität Hannover, Callinstrasse 3, 30167 Hannover, Germany*

Corresponding author**:** Stefano Rossi

e-mail: stefano.rossi1@studenti.unipg.it

Tel.: +39 075 585 2601

Fax: +39 075 585 2603

Abstract

We combined literature and experimental data to determine the role of magma mixing in the pre-eruptive dynamics of the Aeolian Islands volcanoes. As a first step, we systematically reviewed the evidence supporting the hypothesis of mixing-triggered eruptions in the Aeolian archipelago, providing textural, chemical, and rheological constraints. The existing data highlighted the significant role of magma mixing in many eruptions within the Aeolian archipelago. Examples include the Upper Pollara and Porri volcano eruptions at Salina, Monte Guardia, and the AD 1230 Monte Pilato eruption at Lipari, as well as the present-day activity at Stromboli. Then, we focused on Vulcano Island, chosen as a case study because it represents one of the volcanoes posing the highest risk in the Aeolian archipelago. At Vulcano Island, we highlighted the role of magma mixing in the AD 1739 and 1888–90 eruptions. Finally, we investigated mixing-to-eruption timescales for the AD 1739 eruption, performing mixing experiments, and evaluated the progressive decay of the chemical concentration variance with time. Results pointed to mixing-to-eruption timescales of the order of 29±9 h and magma ascent rates ranging between 3×10^{-2} and 5×10^{-2} m s^{-1}. We finally emphasized that the presented results may have significant implications in the context of volcanic hazard mitigation and planning of emergency activities.

Key words: magma mixing, time series experiments, eruption timescales

1. Introduction

The physical and chemical interaction between compositionally different magmas (i.e. magma mixing in the broadest interpretation that includes mingling and mixing, in agreement with Perugini and Poli, 2012) is a widely studied petrological phenomenon (e.g., Anderson, 1976; Sparks et al., 1977; Bateman, 1995; De Rosa et al. 1996; Wiebe, 1994; De Campos et al., 2008; Albert et al., 2015; Wiesmaier et al., 2015) that has been investigated considering either chemical (e.g., Lesher, 1990; Bateman, 1995; Bergantz et al., 2015; Perugini and Poli, 2005; Petrelli et al., 2006, 2011), thermo-dynamical (e.g., Sparks and Marshall, 1986; Snyder, 2000), or rheological approaches (Blake and Fink, 2000; Albert et al., 2015). Moreover, magma mixing has been suggested as an effective eruption trigger (e.g., Sparks et al. 1977; Druitt et al. 2012), and recently, the combination of experimental investigations and the study of volcanic rocks produced by the interaction between different magmas has been proposed as a robust volcanic chronometer (e.g., Perugini et al., 2015). The main idea behind the use of magma mixing as a volcanic chronometer assumes the injection of hotter, more primitive, and potentially volatile-rich magma into a more evolved magmatic reservoir as among the leading causes of mechanical destabilization of the system, possibly triggering the eruption (e.g., Sparks et al., 1977; Eichelberger, 1980; Huppert et al., 1984; Wiebe, 1994; Laumonier et al., 2014a, 2014b; Perugini et al., 2015).

Observation of pyroclastic rocks and lava flows strongly supports the hypothesis that magma mixing is often involved in the volcanic plumbing system (i.e. the structural framework of the pathways and storage regions through which magma travels from its source region to the Earth's surface; Galland et al., 2015) before an eruption. Examples of significant eruptions from the last two centuries providing evidence of magma mixing are Tambora (1815; Gertisser et al., 2011), Mount St. Helens (1980; Gardner et al., 1995), Pinatubo (1991; Pallister et al., 1992), Soufriere Hills (1995; Murphy et al., 1998), and Ejafjallajökull (2010; Sigmundsson et al., 2010). However, even if the occurrence of a direct link between the injection of new magmas in a shallow crust

magmatic reservoir and a subsequent eruption was already established, the timescales of the process remain unclear and warrant further investigation.

Substantial evidence of magma mixing has been found in many pyroclastic and effusive products derived from the eruptive activity of the Aeolian Islands volcanoes (Southern Tyrrhenian Sea, Italy), making this area of great interest to study the interaction between compositionally different magmas prior to the eruptions (Francalanci et al., 1989, 1999; Peccerillo, 2005; Petrone et al., 2006; 2018; De Rosa et al., 1996, 2002).

In this paper, we report a comprehensive review of the evidence supporting the hypothesis of mixing-triggered eruptions in the Aeolian archipelago, providing textural, chemical, and rheological constraints.

Subsequently, we experimentally investigated the AD 1739 eruption at Vulcano Island (Aeolian archipelago), chosen as a case study because it represents one of the most active and dangerous volcanoes in the Aeolian archipelago, posing the highest risk in the region (De Astis et al., 2013). By comparing the results of magma mixing experiments to natural samples, we provide an estimate of the timescales occurring between the beginning of the mixing process in the shallow magmatic reservoir and the subsequent eruption. Finally, we present an estimate of the averaged magma ascent rates, and discuss the implications of the results for an improved definition of the dynamics occurring in the Vulcano plumbing system prior to the eruption.

2. Geological setting and petro-volcanological background

2.1. Geologic summary of the Aeolian archipelago and evidence of magma mixing

The Aeolian Islands are a volcanic archipelago in the Southern Tyrrhenian Sea, north of the coast of Sicily. The archipelago consists of seven islands: Lipari, Stromboli, Vulcano, Salina, Alicudi, Filicudi, and Panarea (Fig. 1A). The subaerial volcanoes of this archipelago and the associated volcanic seamounts form a ring-shaped structure emplaced on continental crust.

The volcanic products (aged from 430 ka to present; Peccerillo, 2005) range from calc-alkaline, high-K calc-alkaline, to shoshonitic and alkaline (Keller, 1980; Peccerillo, 2005; Fig. 2).

The geochemical affinity of these rocks and the occurrence of deep seismicity in the southern sector of the Tyrrhenian Sea connects the genesis of the Aeolian archipelago to the subduction of the Ionian domain beneath the Calabrian arc (Keller, 1980; Peccerillo, 2005).

The mixing process, together with fractional crystallization, magma–fluid interactions, and different degrees of host rock assimilation, has often been invoked as a recurring event in the petrological evolution of magmatic feeding systems throughout the Aeolian arc (e.g., De Rosa et al., 2003; Francalanci et al., 1989; Gioncada et al., 2005; De Astis et al., 2013). Many studies addressing magma mixing have focused on detailed descriptions and analysis of morphological features (De Rosa et al., 1996, 2002, 2003; Perugini et al., 2004, 2007; Ventura et al., 2006; Vetere et al., 2015a) or physicochemical disequilibria in crystals (Landi et al., 2004; Perugini and Poli, 2012). Furthermore, particular emphasis has been given to the study of mafic enclaves dispersed in more felsic magmas, as these occur in several outcrops throughout the Aeolian archipelago (e.g., Pollara depression and Porri lava flow at Salina; La Fossa cone at Vulcano; Monte Guardia and Monte Pilato at Lipari; De Rosa et al., 2003; Perugini et al., 2004, 2007; Piochi et al., 2009; Davì et al., 2009, 2010, Vetere et al., 2015a).

2.2. Vulcano Island and the AD 1739 and 1888–90 *eruptions*

Vulcano is the southernmost island of the Aeolian archipelago and, along with Salina and Lipari, it forms a NNW–SSE-striking volcanic belt deviating from the Aeolian ring-shaped structure (Peccerillo, 2005; Fig. 1B).

The southern part of Vulcano Island is formed by the Primordial Vulcano and Piano Caldera, while the northern sector hosts the Mastro Minico-Lentia complex and the Fossa Caldera (De Astis et al., 2013). The volcanic activity of Vulcano started ca. 120 ka ago (Peccerillo, 2005; Clocchiatti et al., 1994; De Astis et al., 2013; Fig. 1B) and the last eruptions occurred in AD 1739

and 1888–90. The Vulcanello Peninsula, along the northern part of the island, consists of shoshonitic and latitic lava flows. Along with the volcanic products of the La Fossa cone, these products represent the most alkaline compositions found in the Aeolian archipelago (Peccerillo, 2005; De Astis et al., 2013). In particular, the magmatic products from the AD 1739 and 1888–90 eruptions range from latitic to rhyolitic compositions (Peccerillo, 2005; Clocchiatti et al., 1994; highlighted in red as probability density function in Fig. 2A).

Two different phases characterize the AD 1739 eruption. The early explosive phase was essentially phreatomagmatic. It produced several low-energy pyroclastic density currents (PDCs) and minor fallout episodes (De Astis et al., 2013). The deposits generated during this phase are prevalently exposed along the flanks of La Fossa cone and are interlayered with banded pumiceous trachy-rhyolitic bombs.

The subsequent effusive phase produced the Pietre Cotte lava flow (Fig. 3A). It represents the latest lava flow event at Vulcano Island and shows evidence of magma mixing through the presence of mafic enclaves in a rhyolitic host (Piochi et al., 2009). Detailed observations suggest that the mafic enclaves constitute 5–7% of the entire outcrop and their presence led to the interpretation of the occurrence of magma mixing during the eruptive event (Perugini et al., 2007).

The AD 1888–90 eruption represents the latest activity of La Fossa (Clocchiatti et al., 1994; De Astis et al., 2013). The initial eruptive phases are recorded in the stratigraphic sequence by rhyolitic phreatomagmatic breccias containing magmatic enclaves (latitic in composition). The following phases were predominantly explosive and consisted of pyroclastic surges and intermittent fallout products ranging from trachytic to latitic. The upper sequence is characterized by rhyolitic tephra, similar in composition to the initial eruptive phase (Clocchiatti et al., 1994; De Astis et al., 2013). The occurrence of magma mixing is highlighted by reaction rims in the different phases, reversely zoned clinopyroxenes, banded pyroclastic products, and the presence of magmatic enclaves (latitic in composition). Clocchiatti et al. (1994) fixed the maximum volume of the latitic enclaves in the hosting rhyolite to ~10%.

The estimated temperature for mixing processes, which occurred in a shallow reservoir (~ 1 kbar; De Astis et al., 2013) for both the AD 1739 and 1888–90 events, is 1000–1100°C for the latite and 955–1000°C for the rhyolite, in agreement with Vetere et al. (2015a) and Clocchiatti et al. (1994), respectively. To achieve such conditions, the volumetric proportions of latitic magma involved in the re-heating of the shallow magmatic reservoir were assumed to be significantly higher than the amount shown by field observations as reported by Vetere et al. (2015a). This observation also agrees with the experimental results reported by Laumonier et al. (2014b), stating that onset of mixing in a felsic reservoir (e.g., rhyolitic or dacitic) requires a mass fraction of mafic magma of approximately 60–65% (Laumonier et al., 2014b).

3. Methodology

3.1. Experimental end-members and banded pumices

The utilized end-members were sampled by the Petro-Volcanology Research Group (PVRG; http://pvrg.unipg.it), University of Perugia. The least evolved was a latite sampled from the top part (AD 1888–90 eruption) of the La Fossa cone, while the most evolved was a high-K rhyolitic obsidian from the Pietre Cotte lava flow (AD 1739 eruption). The choice of the end-members was determined by field observations and geochemical modeling of whole-rock analysis pointing to these compositions as end-members for the mixing process occurring before the AD 1739 eruption (Clocchiatti et al., 1994; Piochi et al., 2009; Vetere et al., 2015a).

The rhyolitic end-member (i.e. felsic; Fig. 3B) is characterized by a banded aspect with an alternation of pumiceous and glassy bands with elongation parallel to the lava flow direction (Vetere et al., 2015a).

The latitic end-member (i.e. mafic; Fig. 3C) appears as a dark gray rock showing a high degree of vesiculation. It occurs as enclaves within the rhyolitic host. Petrographically, it shows a porphyritic texture with euhedral to sub-euhedral crystals of clinopyroxene and plagioclase

175 immersed in a microcrystalline groundmass composed of clinopyroxene, plagioclase, opaque
176 minerals, and glass.

177 Fig. 4 shows the composition of the end-members plotted in a total-alkali vs. silica diagram
178 (TAS, Le Maitre, 1989) in which the literature data for Vulcano Island are also reported.

179 Banded pumices, utilized to compare the experimental results to natural samples, are from
180 the fallout events of the early explosive phase of the AD 1739 eruption (Fig. 3D). Macroscopically,
181 they show a high degree of vesiculation along with the presence of several filament-like structures.
182 Optical analysis showed a glassy matrix with a few occurrences of small phenocrysts (mode <2%),
183 mainly plagioclase, clinopyroxene, and minor olivine. The collected banded pumices did not
184 highlight significant inter-sample textural and compositional variations. Because of these
185 similarities, we selected one representative sample to be utilized in the present study. The sample
186 was prepared for a 100-μm thin section and polished using up to 1-μm diamond pastes for the
187 analysis via electron microprobe.

188

189 *3.2. Experimental apparatus and methods*

190 To provide mixing-to-eruption timescales, new magma mixing experiments were performed
191 using the Chaotic Magma Mixing Apparatus (COMMA, Morgavi et al., 2015) installed at the
192 Department of Physics and Geology, University of Perugia (Italy). The device was designed to
193 conduct experiments at high temperature with high-viscosity (up to 10^6 Pa s) natural and synthetic
194 magmas up to a temperature of 1800°C (Fig 5; Morgavi et al., 2015).

195 The apparatus produces chaotic flow dynamics in the mixing system using a stirring
196 protocol known as a Journal Bearing System (JBS; Swanson and Ottino, 1990). The ability of the
197 JBS to produce efficient mixing patterns, by fully controlling the mixing kinematics, makes it well
198 suited for the experimental investigation of magma mixing processes (De Campos et al., 2008,
199 2011; Morgavi et al., 2015; Rossi et al., 2017). The utilized mixing protocol produces textures
200 representative of several natural examples bearing evidence of magmatic interaction, among which

many cases have been documented in the Aeolian Islands (De Rosa et al., 2002; Perugini et al., 2004; Perugini and Poli, 2012). Therefore, it allows one to reproduce the non-linear nature of the mixing process (e.g., chaotic; Flinders and Clemens, 1996; De Rosa et al., 2002). In addition, the aforementioned cited study cases support the robustness of the assumption that chaotic mixing experiments can accurately reproduce pre-eruptive magma mixing events (De Campos et al., 2008, 2011; Perugini et al., 2015).

The system is composed of a $Pt_{80}Rh_{20}$ crucible (i.e. the outer cylinder) that contains the two end-member compositions and an inner, off-centred spindle (i.e. the inner cylinder; Fig. 5). The geometry of the system is determined by two parameters: (a) the ratio of the radii of the two cylinders $r = R_{in}/R_{out} = 1/3$ and (b) the eccentricity ratio of the outer cylinder $\varepsilon = \delta/R_{out} = 0.3$, where δ is the distance between the centers of the two cylinders (Swanson and Ottino, 1990). The mixing of magmas is triggered by the alternating rotations of the inner and the outer cylinder in opposite directions because both streamlines and velocity are time-dependent (Galaktionov et al., 2002; Swanson and Ottino, 1990). For the present work, the characteristic velocity $V = |V_{in}| + |V_{out}|$ and characteristic length $L = R_{out} - R_{in}$ are equal to 2.8×10^{-5} m s^{-1} and 1.23×10^{-2} m, respectively, with a strain rate of ~10^{-3} s^{-1}, calculated in agreement with Galaktionov et al., 2002.

During the experiments, the relative volumes of the felsic (rhyolite) and mafic (latite) end-members were 88% and 12%, respectively. Notably, the volumetric proportions used in the experimental setup were relevant to those observed in the erupted products (Perugini et al., 2007; Clocchiatti et al., 1994), although the volumetric balances in the magmatic reservoir were reasonably different with much greater volume of the less-evolved end-member being intruded (see also section 2.2).

The durations of the two experiments were 10.5 h (Experiment A) and 31.5 h (Experiment B), corresponding to one and three repetitions of a protocol consisting of two rotations of the crucible over 7 h and six rotations of the spindle over 3.5 h, respectively. The experiment started

with two homogeneous contrasting multicomponent silicate melts. With time, the initial elemental concentrations in the end-members were expected to drift towards the hybrid of the system.

The experimental conditions were P = 1 atm and T = 1200°C. The choice of 1200°C for the experiments aimed at compensating for the absence of water during the experiments performed at atmospheric pressure, resulting a rheological and chemical behaviour similar to the natural occurrence (H_2O ~1.5 wt.%; T ~1000°C; P ~ 1 kbar; Clocchiatti et al., 1994). In particular, we utilized a parametrization for the viscosity (η) and the chemical diffusivities based on the models of Giordano et al. (2008) and González-García at al. (2017), respectively. In detail, Fig. 6 shows the parametrization for the viscosity based on the model of Giordano et al. (2008). For both the latitic and rhyolitic end-members, the value of η in the presence of ~1.5 wt.% H_2O at T=1000°C (i.e. the estimated temperature for the AD 1739 eruption) agrees with the parametrization of η for dry melts at the experimental temperature (i.e. 1200°C). For the chemical diffusivities, the presence of ~1.5 wt.% of water leads to an increase in the chemical diffusivities of ~1.5 log units compared to that of dry conditions (González-García at al., 2017). Assuming an Arrhenian behaviour for the selected chemical species (e.g., Zhang et al., 2010), an increase in the temperature of ~200°C well agrees well with an increase in the chemical diffusivities of ~1.5 log units.

The temperature inside the experimental sample was monitored using an S-type Pt/Pt-Rh thermocouple. The error for the temperature was ± 3°C.

At the end of each experiment, the furnace was rapidly moved downward to allow the experimental sample to be near the cooling heads positioned at the top and the bottom exits of the furnace tube. To ensure the achievement of a glassy sample, we calculated the NBO/T value in agreement with Mysen and Richet (2005) for the latitic composition (i.e. the experimental composition in which the development of crystals preferentially occurs in the studied system). The resulting value was 0.27. Starting from the obtained NBO/T value, we calculated the critical cooling rate (Rc) as ca. 4000 °C/h, according to Vetere et al., (2015b). During the quenching, the temperature of the samples decreased from 1200°C to 665°C (Tg for our composition calculated

252 after Giordano et al., 2008) in ca. 3 min, corresponding to a quench rate of ~10^4 °C/h, significantly
253 higher than the obtained Rc. This rate completely suppressed nucleation and crystallization
254 processes within the experimental samples. The sample was then cored out from the outer cylinder,
255 set in epoxy resin, and left to harden for 24 h. Ultimately, the experimental product was cut into
256 slices ca. 4 mm in thickness and polished using up to 1-μm diamond pastes for analysis using an
257 electron microprobe.
258
259 *3.3. Analytical methods*
260 Major element concentrations and back-scattered electron (BSE) images were acquired
261 using a Cameca SX100 electron microprobe (EMP) at the Institüt für Mineralogie, Leibniz
262 Universität Hannover (Germany). The operating conditions were characterized by an acceleration
263 voltage of 15 kV, a beam current of 4 nA, and a beam diameter of 10 μm to minimize the alkali loss
264 in the glass analysis. Raw data were converted to concentration using the software "Peak Sight" and
265 "PAP" matrix (Pouchou and Pichoir, 1991). The reference materials utilized for the calibration were
266 wollastonite for Ca and Si, periclase for Mg, hematite for Fe, corundum for Al, rutile for Ti,
267 orthoclase for K, and albite for Na. The counting time was 10 s for each element.
268 Accuracy and precision were determined for the VG-568 (rhyolite) and VG-2 (basalt)
269 glasses (Jarosewich et al., 1980), utilized as secondary reference materials. Absolute analytical
270 errors, measured for international reference materials, were of the order of 4% for all analyzed
271 elements. During the experiments, a total of five profiles (two for experiment A and three for
272 experiment B) were obtained with a spacing of 15 μm between the analysis points, for a total of 877
273 analytical determinations. The same analytical conditions were used for the three transects
274 performed on the banded pumice, for a total of 92 analytical determinations.
275
276 *3.4. Mixing to Eruption Timescales estimate*

Mixing-to-eruption timescale estimates were developed using the method of concentration variance decay (CVD; Perugini et al., 2015). It was utilized to capture the time elapsing between the beginning of the mixing process (i.e. the injection of new mafic magma in the reservoir) and the eruption. It consisted of experimentally evaluating the rate at which the concentration variance of the different chemical elements decayed with time during the mixing process (e.g., Perugini et al., 2015). The successive step consisted of the derivation of empirical relations, typically exponential, linking the variance decay with time. Finally, comparing the concentration variances of the natural sample, namely the banded pumice generated by the fallout events of the early explosive phase of the AD 1739 eruption (Fig. 3D), to the parametrization derived from the experiments, we provided an estimate of the mixing-to-eruption timescales.

3.4.1. Concentration variance and concentration variance decay

In the fluid dynamics literature, concentration variance is commonly used to evaluate the degree of homogenization in fluid mixtures (e.g., Rothstein et al., 1999). For a given chemical element, the concentration variance is defined as follows:

$$\sigma^2(C^i) = \frac{\sum_{n=1}^{N}(C_n^i - \mu^i)}{N} \quad (1)$$

where N is the number of the analytical determinations, C_n^i is the concentration of a given chemical element i in the analytical determination n, and μ^i is the average composition for the element i. The concentration variance is strongly dependent on the mixing time: when the mixing time increases and the system moves towards homogeneity, the concentration variance progressively decreases. Moreover, $\sigma^2(C^i)$ depends on the concentrations of each element i.

In this work, considering the concentration of chemical elements in the experimental sample reported in Table 1 and following the method of Perugini et al. (2015), we normalized the variance values to the initial variance utilizing the following equation:

$$\sigma_n^2(C^i) = \frac{\sigma^2(C^i)_t}{\sigma^2(C^i)_{t=0}} \quad (2)$$

where $\sigma^2(C^i)_t$ and $\sigma^2(C^i)_{t=0}$ are, respectively, the variance in the chemical element (C^i) at time t and $t = 0$ (i.e. before the beginning of the experiment or mixing event in nature).

In detail, a concentration variance (σ_n^2) was calculated for all the investigated chemical elements in each analyzed transect. The operation was repeated for the two-mixing times (i.e. 10.5 h and 31.5 h). The obtained values were subsequently averaged to obtain a representative estimation of the homogenization degree in the studied system.

In addition, using the same procedure, we calculated the σ_n^2 for the natural sample (the banded pumice sampled from the fallout deposits of the AD 1739 eruption). Hereafter, we always refer to the concentration variance considering Eq. (2).

The concept of concentration variance decay (CVD) was used in Perugini et al. (2015) and Rossi et al. (2017) in the assessment of the elemental mobility and chemical homogenization of silicate melt systems. Particularly, for all the analyzed chemical elements, the CVD is modeled by an exponential law as follows:

$$\sigma_n^2(C^i) = C_0 exp(-Rt) + C_1 \quad (3)$$

where C_0 and C_1 represent the value of the concentration variance $[\sigma_n^2(C^i)]$ at $t = 0$ and $t = \infty$, respectively, and t is the mixing time. The fitting parameter R is termed the "relaxation of concentration variance" (RCV) and quantifies the rate at which the concentration variance decays with increasing mixing time and, in addition, the mobility of the chemical elements in the system. Regarding the mobility of the chemical elements, the main controlling parameters in a melt are the temperature, chemical composition, volatile content, oxygen fugacity, and pressure (e.g., Zhang et al., 2010). In addition the R parameter accounts, in a single variable, for a range of processes affecting elemental mobility including the (a) partitioning of the chemical elements into different melts (Watson, 1976), (b) influence of advection on apparent diffusive fluxes (Perugini et al., 2006), (c) dependence of diffusivities on multicomponent composition (e.g., Zhang et al., 2010),

and (d) potential development of “uphill” or “downhill” diffusion processes (Watson and Jurewicz, 1984).

4. Results and Discussion

4.1. Evidence linking magma mixing to the eruptive events of the Aeolian archipelago

The main significant points resulting from the review of current literature highlighted that i) magma mixing has been widely documented for most of the eruptions occurring in the Aeolian Islands, ii) many studies have linked the mixing process to an eruption, iii) many works have noted the rapid remobilization of a shallow reservoir prior to an eruption (Table 2 and references therein). In the following, we report the main findings resulting from the investigation of literature data.

At Salina Island, the interaction between a dacitic and a basaltic-andesite magma has been shown by the presence of magmatic enclaves in the Porri lava flow (ca. 43 ka; De Rosa et al., 1996; Ventura et al., 2006) and in products from the Upper Pollara eruption (ca. 13 ka; Perugini et al., 2004). In detail, Perugini et al. (2004) underlined that the analysis of concentration patterns of heterogeneous juvenile products allows for the estimation of initial magma concentrations, and also providing constraints for pre- and syn-eruptive dynamics. In addition, Perugini et al. (2004) interpreted the whole eruptive sequence as the result of the emptying of the whole magmatic reservoir, highlighting that the flow regime during the interaction between the two end-members was heterogeneous, from sub-turbulent to completely turbulent, just prior to and during the eruption.

Regarding the Porri lava flow, De Rosa et al. (1996) and Ventura et al. (2006) reported its structural and geochemical features with evidence of the interaction between two different magmas. They utilized the mixing structures (e.g., enclaves and bandings) to calculate the shear strain of the lava flow and to evaluate the efficiency of the process (De Rosa et al., 1996). Particularly, Ventura et al. (2006) made inferences on the degree of interaction between the different magmas on the basis of the spatial distribution of the enclaves. According to this hypothesis, host magmas

characterized by a homogeneous spatial distribution of enclaves are indicative of efficient advection processes that may favor magma mixing. In contrast, host magmas characterized by an inhomogeneous distribution of enclaves suggest a low dynamical interaction between the two end-members, and therefore inefficient mixing (Ventura et al., 2006).

At Lipari, the juvenile material recognized in the products of the Monte Guardia rhyolitic eruption (ca. 22 ka) was investigated by petrographic, mineralogical and melt inclusion-based studies (De Rosa et al., 2003). Results highlighted that different mixing textures were produced in a single mixing event before the first stage of the eruption, followed by a second phase characterized by a larger volume of magma of rhyolitic composition (De Rosa et al., 2003). Moreover, chemical analysis of zoned clinopyroxenes and plagioclases found in these rocks (Gioncada et al., 2005) support the idea that the chemical zonation in the minerals preceded the eruptive event, with a residence time before mixing on the order of decades to hundreds of years (Gioncada et al., 2005).

Additionally, Davì et al. (2009, 2010) focused on latitic enclaves found in the rhyolitic lava flow of Rocche Rosse, produced by the AD 1230 Monte Pilato eruption. The estimated viscosities were then applied to rheological modeling of mixing processes between the latitic and rhyolitic magmas at conditions relevant for the Rocche Rosse eruption. Results suggested rapid ascent events, occurring just after the beginning of the mixing process (Davì et al. 2009, 2010).

At Stromboli, magma mixing has been widely investigated by several authors (Francalanci et al., 1989, 2012; Petrone et al., 2006, 2018; Armienti et al., 2007; Landi et al., 2004). Mineralogical and chemical studies of lavas and pyroclastic products produced during the 1985–2000 and 2002–2003 eruptions highlighted mixing-related chemical zoning in plagioclase phenocrysts (Landi et al., 2004, 2009). In detail, evidence suggested recharge events in the magmatic system by hotter magma batches. These mixing events, often developing between magmas of similar mafic composition, efficiently occurred in the Stromboli feeding system just before the eruptions during the period 1985–2000 as highlighted by the disequilibrium textures in

the plagioclase phenocrysts (showing an alternation of labradoritic and bytownitic layers; Landi et al., 2004, 2009).

Textural evidence of magma mixing was also reported by Armienti et al. (2007), defining significant chemical zoning and resorption textures in plagioclase, olivine, and pyroxene crystals. In particular, a crystal size distribution analysis suggested a stationary crystallizing system being continuously re-injected by crystal-free basaltic melt (Armienti et al., 2007). In addition, the large radiogenic isotope (Sr, Nd, Pb, U, and Th) variations detected in the plagioclase, olivine, and clinopyroxene (Francalanci et al., 1999, 2012; Landi et al., 2009) confirmed the occurrence of mixing processes between the crystal-rich and crystal-poor magmas in a shallow magmatic reservoir (Francalanci et al., 2012). Moreover, Petrone et al. (2006) highlighted oscillatory patterns and sharp compositional changes in clinopyroxene and plagioclase phases, suggesting complex dynamics in the magmatic reservoir. Petrone et al. (2006) also suggested the injection of mafic magma batches into the magmatic reservoir, highlighting that magma mixing played a significant role in the development of compositional changes and temperature variations (Petrone et al., 2006). Recently, Petrone et al. (2018) estimated the residence times of mafic magmas in the volcanic feeding systems of the Post-Pizzo pyroclastic sequence (ca. 1.7–1.5 ka) and Early Paroxysms of the present eruptive sequence using Fe–Mg diffusion in clinopyroxenes. They provided timescales of the order of 1 to approximately 50 years between the arrival of the mafic magma in the shallow system and the eruption (Petrone et al., 2018). In addition, modeling provided by Petrone et al. (2018) highlighted mixing-to-eruption timescales from days to months for selected clinopyroxenes, further suggesting that rapid mixing events and short storage timescales are key parameters in the pre-eruptive dynamics of the system. Many authors noted the evidence that the present-day activity of Stromboli is controlled by a steady-state feeding system in which injection, mixing, degassing, and crystallization at a shallow level continuously occur (Francalanci et al., 1999, 2012; Landi et al., 2009; Petrone et al., 2006, 2018). Moreover, Landi et al. (2009) suggested that the change between strombolian and effusive activity is mainly related to periods of relatively more or less

403 vigorous injection into the shallow magmatic system (Landi et al., 2009). As a summary, Table 2
404 reports a synthesis of the evidence linking the mixing process to the eruptive events of the whole
405 Aeolian archipelago.
406
407 *4.2. Evidence linking magma mixing to the AD 1739 and 1888–90 eruptions of Vulcano Island*
408 The process of magma mixing in the AD 1739 eruption of Vulcano Island has been widely
409 investigated (Perugini et al., 2007; Piochi et al., 2009; Vetere et al., 2015a), focusing on the
410 morphological, geochemical thermo-dynamical, and rheological characterization of the erupted
411 magmas.
412 All the studies noted the mixing process as having a primary role in the pre-eruptive
413 evolution of the volcanic plumbing system, and also suggesting a direct link between the occurrence
414 of magma mixing and the subsequent eruption. In detail, Perugini et al. (2007) quantitatively
415 investigated the morphology and size distributions of the enclaves in the Pietre Cotte lava flow.
416 Perugini et al. (2007) showed that the enclaves resulted from the fragmentation of viscous fingering
417 structures following the injection of mafic magma into a felsic reservoir just prior to the eruption. In
418 addition, geochemical investigations performed by Piochi et al. (2009) provided evidence that the
419 latitic enclaves and the rhyolitic host magma were subject to similar thermo-barometric conditions,
420 further supporting the idea of the coexistence of compositionally variable magmas in the shallow
421 magmatic reservoir beneath the La Fossa cone before the AD 1739 eruption.
422 Vetere et al. (2015a), using thermo-dynamical and rheological constraints, suggested that the
423 most plausible scenario for the AD 1739 eruption was a shallow reservoir in which a latitic magma
424 intruded a rhyolitic magma, finally leading to eruptive events. Part of the volume of the latitic
425 magma remained in the reservoir after the conclusion of the AD 1739 eruptive event, to be erupted
426 during the last cycle of AD 1888–90.
427 In the case of the AD 1888–90 eruptive cycle, Clocchiatti et al. (1994), utilizing whole-rock
428 analysis and isotopic investigations, highlighted that the erupted pyroclastic products were derived

429 from mixing between a rhyolitic end-member and a latite of similar composition to the enclaves
430 detected in the Pietre Cotte lava flow. In addition, Clocchiatti et al. (1994) highlighted a direct link
431 between the mixing process, occurring in the shallow reservoir, and the subsequent eruption. In
432 detail, Clocchiatti et al. (1994) suggested the unlocking of the rhyolite by re-heating resulting from
433 the injection of the hotter latite.
434
435 *4.3 Timescale estimation for the AD 1739 eruption*
436 The presented magma mixing experiments aimed to define the mixing-to-eruption
437 timescales, i.e. the time elapsed between the beginning of the mixing in the magmatic reservoir and
438 the subsequent eruption, for the AD 1739 eruption at Vulcano island.
439 The morphological results of the experiments are shown in Fig. 7, displaying BSE images of
440 selected portions of the experimental products in which the presence of stretched and folded
441 alternating filaments of the two end-members are clearly observable. The density of the filament
442 populations as well as their thicknesses strongly vary throughout the whole experimental product as
443 a direct consequence of the complex dynamics acting during the mixing process (i.e. the JBS
444 protocol; Swanson and Ottino, 1990).
445 The analysis performed using EMP on the experimental and natural samples is shown in
446 Table SM1. Fig. 8 shows the compositional variation of all the analyzed elements of the
447 experimental products (i.e. Al_2O_3, CaO, MgO, K_2O, FeO, Na_2O, and TiO_2) vs. SiO_2. End-member
448 compositions are also reported, as a reference.
449 Fig. 9 shows the evolution of the normalized concentration variance, i.e. $\sigma_n^2(C^i)$, in the
450 experiments as a function of time. In addition, Fig. 9 shows the results of the exponential fitting,
451 linking the evolution of the normalized variance and time (please refer to section 3.4.1. for further
452 details). Results highlight that the investigated elements (i.e. Si, Mg, Ca, Ti, Fe, Na, Al, and K)
453 show rates of decay, measured by the *R* parameter, ranging between 0.122 and 0.185 (Fig. 9).

Furthermore, Fig. 10 shows the variability in all the analyzed elements (i.e. Si, Mg, Ca, Ti, Fe, Na, Al, and K) along transects made for the analyzed banded pumice used in this work as natural sample, representative of the explosive phase of the AD 1739 eruption. The banded pumice highlights compositions ranging between trachyte (i.e. SiO_2 ~ 68 wt.%) and rhyolite (i.e. SiO_2 ~ 73 wt.%; Fig. 10). These compositions agree well with those produced by the mixing process between the latitic (i.e. SiO_2 ~ 58 wt.%) and rhyolitic (i.e. SiO_2 ~ 74 wt.%) end-members utilized during the experiments, in the proportions reported in the present study (i.e. 12–88%).

As for the experimental products, the normalized variance was also estimated for the natural sample, including all the analyzed elements (i.e. Si, Al, K, Na, Ca, Mg, Fe, and Ti). Mixing-to-eruption timescales were then estimated using Eq. (3). The obtained mixing-to-eruption timescales show a variability ranging from ca. 10 to 39 h (i.e. the minimum and the maximum value, respectively), with an average of 29±9 (s.d.) h (please refer to Table SM2 for further details). The obtained timescales, of the order of days, are very short if compared to the few other estimates for volcanic systems of the Aeolian archipelago ranging from years to decades (e.g., Gioncada et al., 2005 and Petrone et al., 2018). However, they agree with the lower bound of the estimates reported by Petrone et al. (2018), of the order of days to months, for clinopyroxene portions capturing the final stages (i.e. final injections) of the mixing process at Stromboli.

In addition, the recovered mixing-to-eruption timescale estimates can be used to infer the average magma ascent velocity in the case of the AD 1739 eruption of Vulcano Island. To achieve such estimates, the definition of the depth for the final magma storage before the eruption was essential. On the basis of petrological, geochemical, isotopic, and geobarometric data, De Astis et al. (2013) showed that, in the case of the La Fossa cone, the most probable final storage region was at ca. 3–5 km depth.

Assuming 3 and 5 km as the upper and lower boundary for the magmatic storage depths of the AD 1739 eruption and combining them with the mixing-to-eruption timescales (i.e. 29±9 h) reported in the present manuscript, we estimated averaged magma ascent rates ranging from 3×10^{-2}

480 to 5×10^{-2} m s^{-1}. Notably, the obtained ascent rate values are row estimates, and they do not imply
481 any inference regarding modulations of the velocity profile from the storage region to the surface
482 because of potential changes in the physical properties of magma during the ascent or other factors.
483 Finally, Fig. 11 shows the inferred temporal evolution of the shallow magmatic system
484 beneath the La Fossa cone before the AD 1739 eruption. In detail, at the initial time $t = 0$, a
485 rhyolitic reservoir was at ca. 3–5 km. The ascent of the latitic magma from a deeper reservoir (20–
486 25 km; De Astis et al., 2013) produced a re-heating of the rhyolite, triggering the unlocking of the
487 system and the mixing process, lasting for a maximum of ca. 39 h, and finally leading to the AD
488 1739 eruptive event.
489
490 **5. Concluding Remarks**
491 In this work, we extensively reviewed evidence supporting the hypothesis of mixing-
492 triggered eruptions for the Aeolian archipelago, providing textural, chemical, and rheological
493 constraints. Results highlighted a strict relation between the occurrence of magma mixing at
494 shallow crustal levels and the eruptions. In addition, the detailed review of literature data allowed us
495 to improve our understanding regarding pre-eruptive dynamics occurring in the feeding systems of
496 active volcanoes of the Aeolian archipelago.
497 Finally, the performed experiments provided constraints on mixing-to-eruption timescales
498 for the AD 1739 eruption that occurred at Vulcano Island, utilized as a case study. Our results
499 suggest an average mixing-to-eruption time (i.e. the time between the onset of mixing in the
500 reservoir and the eruption) of 29±9 h and magma ascent rates ranging between 3×10^{-2} and 5×10^{-2}
501 m s^{-1}.
502 These new findings may have important implications for volcano monitoring and civil
503 protection purposes. For example, short mixing-to-eruption timescales and high ascent velocities
504 (e.g., Petrelli et al., 2018) for magma rising towards the Earth's surface may imply short warning
505 times for volcanic crises, on the order of days to hours.

Acknowledgments

This research was funded by the European Research Council (ERC) Consolidator Grant ERC-2013-Co-G No. 612776 – CHRONOS to D. Perugini. F. Vetere wishes to acknowledge support from the MIUR-DAAD Joint Mobility Project (57262582). M. Petrelli wishes to acknowledge support from the University of Perugia, Dipartimento di Fisica e Geologia, "CHALLENGE" FRB 2015 grant. Constructive comments by B. Scaillet and S. Kolzenburg are gratefully acknowledged.

References

Albert, H., Perugini, D., Martí, J., 2015. Fractal Analysis of Enclaves as a New Tool for Estimating Rheological Properties of Magmas During Mixing: The Case of Montaña Reventada (Tenerife, Canary Islands). Pure and Applied Geophysics 172, 1803-1814.

Anderson, A.T., 1976. Magma mixing: petrological process and volcanological tool. Journal of Volcanology and Geothermal Research 1, 3–33.

Aparicio, A., Frazzetta, G., 2008. Magma mixing in Vulcanello (Vulcano Island, Italy). Estudios Geológicos 64, 5-16.

Armienti, P., Francalanci, L., Landi, P., 2007. Textural effects of steady state behaviour of the Stromboli feeding system. Journal of Volcanology and Geothermal Research 160, 86-98.

Bateman, R., 1995. The interplay between crystallization, replenishment and hybridization in large felsic magma chambers. Earth-Science Reviews 39, 91–106.

Bergantz, G.W., Schleicher, J.M., Burgisser, A., 2015. Open-system dynamics and mixing in magma mushes. Nature Geoscience 8 (10), pp. 793-796.

Blake, S., Fink, J.H., 2000. On the deformation and freezing of enclaves during magma mixing. Journal of Volcanology and Geothermal Research 95, 1-8.

530 Clocchiatti, R., Del Moro, A., Gioncada, A., Joron, J.L., Mosbah, M., Pinarelli, L., Sbrana, A.,
531 1994. Assessment of a shallow magmatic system: the 1888–90 eruption, Vulcano Island, Italy.
532 Bulletin of Volcanology 56, 466–486.

533 Davì, M., De Rosa, R., Donato, P., Vetere, F., Barca, D., Cavallo, A., 2009. Magmatic Evolution
534 and plumbing system of ring-fault volcanism: the Vulcanello Peninsula (Aeolian Islands,
535 Italy). European Journal of Mineralogy 21, 1009–1028.

536 Davì. M., De Rosa. R., Holtz. F., 2010. Mafic enclaves in the rhyolitic products of Lipari historical
537 eruptions: relationships with the coeval Vulcano magmas (Aeolian Islands, Italy). Bulletin of
538 Volcanology 72 (8), 991-1008.

539 De Astis, G., La Volpe, L., Peccerillo, A., Civetta, L., 1997. Volcanological and petrological
540 evolution of Vulcano island (Aeolian Arc, southern Tyrrhenian Sea). Journal of Geophysical
541 Research: Solid Earth 102, 8021–8050.

542 De Astis, G., Lucchi, F., Dellino, P., La Volpe, L., Tranne, C.A., Frezzotti, M.L., Peccerillo, A.,
543 2013. Geology, volcanic history and petrology of Vulcano (central Aeolian archipelago),
544 Chapter 11. Geological Society of London, Memoirs 2013, 281-349.

545 De Campos, C.P., Dingwell, D.B., Perugini, D., Civetta, L., Fehr, T.K., 2008. Heterogeneities in
546 magma chambers: insights from the behavior of major and minor elements during mixing
547 experiments with natural alkaline melts. Chemical Geology 256, 131-145.

548 De Campos, C.P., Perugini, D., Ertel-Ingrisch, W., Dingwell, D.B., Poli, G., 2011. Enhancement of
549 magma mixing efficiency by chaotic dynamics: an experimental study. Contributions to
550 Mineralogy and Petrology 161, 863-881.

551 De Rosa, R., Mazzuoli, R., Ventura, G., 1996. Relationships between deformation and mixing
552 processes in lava flows: A case study from Salina (Aeolian Islands, Tyrrhenian Sea). Bulletin

553 of Volcanology 58, 286–297.

554 De Rosa, R., Donato, P., Ventura, G., 2002. Fractal analysis of mingled/mixed magmas: an example
555 from Upper Pollara eruption (Salina Island, Southern Thyrrhenian Sea). Lithos 65, 299-311.

556 De Rosa, R., Donato, P., Gioncada, A., Masetti, M., Santacroce, R., 2003. The Monte Guardia
557 eruption (Lipari, Aeolian Islands): an example of a reversely zoned magma mixing sequence.
558 Bulletin of Volcanology 65, 530-543.

559 Druitt, T.H., Costa, F., Deloule, E., Dungan, M. & Scaillet, B., 2012. Decadal to monthly timescales
560 of magma transfer and reservoir growth at a caldera volcano. Nature, 482, 77-97.

561 Eichelberger, J.C., 1980. Vesiculation of mafic magma during replenishment of silicic magma
562 reservoir. Nature, 288, 446-450.

563 Esperança, S., Crisci, G.M., De Rosa, R., Mazzuoli, R., 1992. The role of the crust in the magmatic
564 evolution of the island of Lipari (Aeolian Islands, Italy). Contributions to Mineralogy and
565 Petrology 112, 450-462.

566 Flinders, J., Clemens, J.D., 1996. Non-linear dynamics, chaos, complexity and enclaves in granitoid
567 magmas. Transactions of the Royal Society of Edinburgh Earth Sciences 87, 217–223.

568 Francalanci, L., Manetti, P., Peccerillo, A., 1989. Volcanological and magmatological evolution of
569 Stromboli volcano (Aeolian Islands): the roles of fractional crystallization, magma mixing,
570 crustal contamination and source heterogenity. Bulletin of Volcanology 51, 355-378.

571 Francalanci, L., Tommasini, S., Conticelli, S., Davies, G.R., 1999. Sr isotope evidence for new
572 magma input and short residence time in the XX century activity of Stromboli volcano. Earth
573 and Planetary Science Letters 167, 61-65.

574 Francalanci, L., Avanzinelli, R., Nardini, I., Tiepolo, M., Davidson, J.P., Vannucci, R., 2012.
575 Crystal recycling in the steady-state system of the active Stromboli volcano: A 2.5-ka story

576 inferred from in situ Sr-isotopeand trace element data. Contributions to Mineralogy and
577 Petrology 163, 109-131.

578 Galaktionov, O.S., Anderson, P.D., Peters, G.W.M., Meijer, H.E.H., 2002. Mapping approach for
579 3D laminar mixing simulations: application to industrial flows. International Journal for
580 Numerical Methods in Fluids 40, 345–351.

581 Galland O., Holohan E., van Wyk de Vries B., Burchardt S., 2015. Laboratory modelling of oolcano
582 plumbing systems: a review. In: Breitkreuz C., Rocchi S. (eds), Physical Geology of Shallow
583 Magmatic Systems. Advances in Volcanology, Springer. doi: 10.1007/11157_2015_9.

584 Gardner, J.E., Rutherford, M., Carey, S., Sigurdsson, H., 1995. Experimental constraints on pre-
585 eruptive water contents and changing magma storage prior to explosive eruptions of Mount St
586 Helens volcano. Bulletin of Volcanology 57, 1-17.

587 Gertisser, R., Self, S., Louise, E.T., Handley, H.K., Van Calsteren, P., Wolff, J.A., 2011. Processes
588 and timescales of magma genesis and differentiation leading to the great Tambora eruption in
589 1815. Journal of Petrology 53, 271-297.

590 Gioncada, A., Mazzuoli, R., Bisson, M., Pareschi, M.T., 2003. Petrology of volcanic products
591 younger than 42 ka on the Lipari-Vulcano complex (Aeolian Islands, Italy): an example of
592 volcanism controlled by tectonics. Journal of Volcanology and Geothermal Research 122, 191-
593 220.

594 Gioncada, A., Mazzuoli, R., Milton, A.J., 2005. Magma mixing at Lipari (Aeolian Islands, Italy):
595 insights from textural and compositional features of phenocrysts. Journal of Volcanology and
596 Geothermal Research 145, 97-118.

597 Giordano, D., Russell, J.K., Dingwell, D.B., 2008. Viscosity of magmatic liquids: a model. Earth
598 and Planetary Science Letters 271, 123-134.

González-García, D., Behrens, H., Petrelli, M., Vetere, F., Morgavi, D., Zhang, C., Perugini, D., 2017. Water-enhanced interdiffusion of major elements between natural shoshonite and high-K rhyolite melts. Chemical Geology 466, 86-101.

Huppert, H.E., Sparks, R.S.J., Turner, J.S., 1984. Some effects of viscosity on the dynamics of replenished magma chambers. Journal of Geophysical Research 89, 6857-6877.

Jarosewich, E.J., Nelen, J.A., Norberg, J.A., 1980. Reference samples for electron microprobe analyses. Geostandards Newsletter 4(1), 43-47.

Keller, J., 1974. Petrology of some volcanic rock series of the Aeolian arc, Southern Tyrrhenian Sea: Calc-alkaline and shoshonitic associations. Contributions to Mineralogy and Petrology 46, 29-47.

Keller, J., 1980. The Island of Vulcano. Rendiconti della Società Italiana di Mineralogia e Petrologia 36, 369-414.

Landi, P., Métrich, N., Bertagnini, A., Rosi, M., 2004. Dynamics of magma mixing and degassing recorded in plagioclase at Stromboli (Aeolian archipelago, Italy). Contributions to Mineralogy and Petrology 147, 213-227.

Landi, P., Corsaro, R.A., Francalanci, L., Civetta, L., Miraglia, L., Pompilio, M., Tesoro, R., 2009. Magma dynamics during the 2007 Stromboli eruption (Aeolian Islands, Italy): mineralogical, geochemical and isotopic data. Journal of Volcanology and Geothermal Research 182, 255-268.

Laumonier, M., Scaillet, B., Arbaret, L., Champallier, R., 2014a. Experimental simulation of magma mixing at high pressure. Lithos, 196-197, 281-300.

Laumonier, M., Scaillet, B., Pichavant, M., Champallier, R., Andujar, J., Arbaret, L., 2014b. On the conditions of magma mixing and its bearing on andesite production in the crust. Nature

622 Communications 5, art. no. 6607.

623 Le Maitre, R.W., 1989. A classification of igneous rocks and glossary of terms. Blackwell, Oxford.

624 Lesher, C.E., 1990. Decoupling of chemical and isotopic exchange during magma mixing. Nature
625 344, 235-237.

626 Morgavi, D., Perugini, D., De Campos, C.P., Ertel-Ingrisch, W., Dingwell, D.B., 2013. Time
627 evolution of chemical exchanges during mixing of rhyolitic and basaltic melts. Contributions
628 to Mineralogy and Petrology 166, 615–638.

629 Morgavi, D., Petrelli, M., Vetere, F.P., González-García, D., Perugini, D., 2015. High-temperature
630 apparatus for chaotic mixing of natural silicate melts. Reviews of Scientific Instruments 86,
631 105108, 1-6.

632 Murphy, M.D., Sparks, R.S.J., Barclay, J., Carroll, M.R., Lejeune, A.M., Brewer, T.S., Macdonald,
633 R., Black, S., Young, S., 1998. The role of magma mixing in triggering the current eruption at
634 the Soufriere Hills Volcano, Montserrat, West Indies. Geophysical Research Letters 25, 3433-
635 3436.

636 Mysen, B., Richet, P. 2005. Iron-bearing melts in Silicate Glasses and Melt, Elsevier Science,
637 Amsterdam, Netherlands.

638 Ochs, F.A., Lange, R.A., 1999. The density of hydrous magmatic liquids. Science 283, 1314-1317.

639 Pallister, J.S., Hoblitt, R.P., Reyes, A.G., 1992. A basalt trigger for the 1991 eruptions of Pinatubo
640 volcano? Nature 356, 426-428.

641 Peccerillo, A., Taylor, S.R., 1976. Geochemistry of Eocene calc-alkaline volcanic rocks from the
642 Kastamou area, north Turkey. Contributions to Mineralogy and Petrology 58, 63–81.

643 Peccerillo, A., 2005. Plio-Quaternary Volcanism in Italy. Springer-Verlag, Berlin Heidelberg.

644 Peccerillo, A., Frezzotti, M.L., De Astis, G., Ventura, G., 2006. Modeling the magma plumbing
645 system of Vulcano (Aeolian Islands, Italy) by integrated fluid inclusion geobarometry,
646 petrology and geophysics. Geology 34 (1), 17-20.

647 Perugini, D., Ventura, G., Petrelli, M., Poli, G., 2004. Kinematics significance of morphological
648 structures generated by mixing of magmas: a case study from Salina Island (Southern Italy).
649 Earth and Planetary Science Letters 222, 1051-1066.

650 Perugini, D., Poli, G., 2005. Viscous fingering during replenishment of felsic magma chambers by
651 continuous inputs of mafic magmas: Field evidence and fluid-mechanics experiments. Geology
652 33, 5-8.

653 Perugini, D., Petrelli, M., Poli, G., 2006. Diffusive fractionation of trace elements by chaotic mixing
654 of magmas. Earth and Planetary Science Letters 243, 669–680.

655 Perugini, D., Valentini, L., Poli, G., 2007. Insights into magma chamber processes from the analysis
656 of size distribution of enclaves in lava flows: a case study from Vulcano island (Southern
657 Italy). Journal of Volcanology and Geothermal Research 166, 193-203.

658 Perugini, D., Poli, G., 2012. The mixing of magmas in plutonic and volcanic environments:
659 Analogies and differences. Lithos 153, 261-277.

660 Perugini, D., De Campos, C.P., Petrelli, M., Dingwell, D.B., 2015. Concentration variance decay
661 during magma mixing: a volcanic chronometer. Scientific Reports 5, 14225.

662 Petrelli, M., Perugini, D., Poli, G., 2006. Time-scales of hybridisation of magmatic enclaves in
663 regular and chaotic flow fields: petrologic and volcanologic implications. Bulletin of
664 Volcanology 68, 285-293.

665 Petrelli, M., Perugini, D., Poli, G., 2011. Transition to chaos and implications for time-scales of
666 magma hybridization during mixing processes in magma chambers. Lithos 125, 211–220.

667 Petrelli, M., El Omari, K., Spina, L., Le Guer, G., La Spina, G., Perugini D., 2018. Timescales of
668 water accumulation in magmas and implications for short warning times of explosive
669 eruptions. Nature Communications 9, art no. 770.

670 Petrone, C.M., Olmi, F., Braschi, E., Francalanci, L., 2006. Mineral chemistry profile: a valuable
671 approach to unravel magma mixing processes in the recent volcanic activity of Stromboli,
672 Italy. Periodico di Mineralogia 75, 277-292.

673 Petrone, C.M., Braschi, E., Francalanci, L., Casalini, M., Tommasini, S., 2018. Rapid mixing and
674 short storage timescale in the magma dynamics of a steady-state volcano. Earth and Planetary
675 Science Letters 492, 206-221.

676 Piochi, M., De Astis, G., Petrelli, M., Ventura, G., Sulpizio, R., Zanetti, A., 2009. Constraining the
677 recent plumbing system of Vulcano (Aeolian Arc, Italy) by textural, petrological, and fractal
678 analysis: The 1739 A.D. Pietre Cotte lava flow. Geochemistry, Geophysics, Geosystems 10, 1-
679 28.

680 Pouchou, J.L., Pichoir, F., 1991. Quantitative analysis of homogeneous or stratified microvolumes
681 applying the model "PAP". Electron Probe Quantification, 31-75.

682 Rossi, S., Petrelli, M., Morgavi, D., González - García, D., Fischer, L.A., Vetere, F., Perugini. D.,
683 2017. Exponential decay of concentration variance during magma mixing: robustness of a
684 volcanic chronometer and implications for the homogenization of chemical heterogeneities in
685 magmatic systems. Lithos 286-287, 396-407.

686 Rothstein, D., Henry, E., Gollub, J., 1999. Persistent patterns in transient chaotic fluid mixing.
687 Nature 401, 770-772.

688 Sigmundsson, F., Hreinsdóttir, S., Hooper, A., Árnadottir, T., Pedersen, R., Roberts, M.J.,
689 Óskarsson, N., Auriac, A., Decriem, J., Einarsson, P., Geirsson, H., Hensch, M., Ófeigsson,

690 B.G., Sturkell, E., Sveinbjörnsson, H., Feigl, K.L., 2010. Intrusion triggering of the 2010
691 Eyjafjallajökull explosive eruption. Nature 468, 426-430.

692 Snyder, D., 2000. Thermal effects on intrusion of basaltic magma into a more silicic magma
693 chamber and implications for eruption triggering. Earth and Planetary Science Letters 175,
694 257-273.

695 Sparks, R.S.J., Sigurdsson, H., Wilson, L., 1977. Magma mixing: a mechanism for triggering acid
696 explosive eruptions. Nature, 267, 315-318.

697 Sparks, R.S.J., Marshall, L.A., 1986. Thermal and mechanical constraints on mixing between mafic
698 and silicic magmas. Journal of Volcanology and Geothermal Research 29, 99-124.

699 Swanson, P.D., Ottino, J.M., 1990. A comparative computational and experimental study of chaotic
700 mixing of viscous fluids. Journal of Fluid Mechanics 213, 227-249.

701 Ventura, G., Del Gaudio, P., Iezzi, G., 2006. Enclaves provide new insights on the dynamics of
702 magma mingling: a case study from Salina island (Southern Tyrrhenian Sea, Italy). Earth and
703 Planetary Science Letters 243, 128-140.

704 Vetere, F., Petrelli, M., Morgavi, D., Perugini, D., 2015a. Dynamics and time evolution of a
705 shallow plumbing system: The 1739 and 1888-90 eruptions, Vulcano Island, Italy. Journal of
706 Volcanology and Geothermal Research 306, 74-82.

707 Vetere, F., Iezzi, G., Behrens, H., Holtz, F., Ventura, G., Misiti, V., Cavallo, A., Mollo, S., Dietrich,
708 M. 2015b. Glass forming ability and crystallisation behaviour of sub-alkaline silicate melts.
709 Earth-Science Reviews 150, 25-44.

710 Watson, E.B., 1976. Two-liquid partition coefficients: Experimental data and geochemical
711 implications. Contributions to Mineralogy and Petrology 56, 119–134.

712 Watson, E.B., Jurewicz, S.R., 1984. Behavior of alkalies during diffusive interaction of granitic

xenoliths with basaltic magma. Journal of Geology 92, 121–131.

Wiebe, R.A., 1994. Silicic Magma Chambers as Traps for Basaltic Magmas: The Cadillac Mountain Intrusive Complex, Mount Desert Island, Maine. Journal of Geology 102, 423–437.

Wiesmaier, S., Morgavi, D., Renggli, C.J., Perugini, D., De Campos, C.P., Hess, K.U., Ertel-Ingrisch, W., Lavallee, Y., Dingwell, D.B., 2015. Magma mixing enhanced by bubble segregation. Solid Earth 6, 1007-1023.

Zhang, Y., Ni, H., Chen, Y., 2010. Diffusion data in silicate melts. Reviews in Mineralogy and Geochemistry 72 (1), 311–408.

Figure Captions

Figure 1: A) Schematic map of the Aeolian Islands and B) schematic geological map of Vulcano Island (modified from Peccerillo et al., 2006) showing the main volcanic units and the location of the Pietre Cotte lava flow generated during the effusive phase of the AD 1739 eruption.

Figure 2: A) Total alkali vs. silica diagram (TAS, Le Maitre, 1989) and B) SiO_2 vs. K_2O diagram (Peccerillo and Taylor, 1976) showing the petrology of rocks of the Aeolian Islands. Literature data are taken from Georoc (http:// georoc.mpch-mainz.gwdg.de).

Figure 3: A) View of the Pietre Cotte lava flow; B) and C) end-members used in the mixing experiments (B: rhyolite and C: latite); D) Example of banded pumice produced by the fallout events of the early phase of the AD 1739 eruption used as natural sample in the present work.

Figure 4: Compositions of latitic (blue star) and rhyolitic (red star) end-members used in this work plotted in a total-alkali vs. silica diagram (Le Maitre, 1989). Literature data for Vulcano Island

737 (taken from Georoc, http:// georoc.mpch-mainz.gwdg.de) are also reported.

738

739 Figure 5: Schematic representation (not to scale) of the COMMA (reproduced and slightly modified
740 from Morgavi et al., 2015). A) Complete experimental setup showing the high-temperature
741 furnace, the upper and lower motors for the rotation of the spindle and the crucible hosting the
742 end-member melts, and the positioning of the experimental crucible; B) enlargement of the
743 experimental crucible filled with the end-member compositions; C) section of the crucible
744 perpendicular to its vertical axis showing the relative position of the end-members and the
745 spindle. Geometrical parameters of the used experimental protocol are also shown (see text and
746 Morgavi et al. (2015) for further details).

747

748 Fig. 6: Parametrization for the melt viscosity (η), based on the model of Giordano et al. (2008),
749 elaborated to compensate for the absence of water (1.5 wt.% in natural samples, Clocchiatti et
750 al., 1994) during the mixing experiments at atmospheric pressure. The gray area represents the
751 estimated η values under the physical conditions of the shallow reservoir before the AD 1739
752 eruption (~ 1000°C, ~ 1 kbar) (3.3±0.2 Pa s for latite, and 5.1±0.2 Pa s for rhyolite; Clocchiatti
753 et al., 1994). The blue line represents the calculated η values as a function of temperature. The
754 blue line intersects the gray area at ~1200°C, the experimental temperature.

755

756 Figure 7: BSE images of selected areas of the experimental samples showing the intricate
757 morphologies produced during the mixing experiments. The location of the selected analyzed
758 transects is also reported. Please refer to Morgavi et al. (2013, 2015) for a detailed description
759 of the morphologies produced by JBS.

760

761 Figure 8: Inter-elemental binary diagrams for the analyzed chemical elements (CaO, MgO, K_2O,
762 Na_2O, FeO, Al_2O_3, and TiO_2) vs. SiO_2 showing the compositional variability resulting from

763 chaotic mixing processes during experiment A (10.5 h) and B (31.5 h). End-member
764 compositions are also reported, as a reference.
765
766 Figure 9: Variation in concentration variance as a function of mixing time for the analyzed chemical
767 elements fitted using Eq. (3) (see text). The value of *R* (i.e., the rate at which concentration
768 variance decays with time) is reported for each analyzed element.
769
770 Figure 10: Compositional variation of the analyzed chemical elements (SiO_2, Al_2O_3, CaO, MgO,
771 Na_2O, K_2O, FeO, and TiO_2) along the transects analyzed for the banded pumice. Estimated
772 mixing-to-eruption timescales are reported for each analyzed element. The location of the
773 analyzed transects is also reported.
774
775 Figure 11: Schematic evolution (not to scale) of the shallow magmatic system beneath the La Fossa
776 cone before the AD 1739 eruption. A): The shallow magmatic reservoir is at 3–5 km depth
777 below the La Fossa cone (De Astis et al., 2013). Deeper batches of latitic magma start to rise
778 towards the felsic reservoir. B): At $t = 0$, the injection of a latitic magma into the rhyolitic
779 reservoir leads to the unlocking of the system and the chemo-physical interaction of the two
780 compositionally different magmas. C) After $t \geq 29$ h, the mixed magma reaches the surface
781 triggering the eruption.
782
783 **Table Captions**
784 Table 1: Concentrations (in weight %) and relative standard deviations of major elements in the
785 felsic and mafic end-member glasses used during the mixing experiments. The value *N*
786 represents the total number of analytical points averaged to obtain the reported concentrations.
787 The density (Ochs and Lange, 1999) and viscosity (Giordano et al., 2008) of both end-

members are also reported.

Table 2: Summary of the most relevant features (discussed in this work) detected in the rocks of the Aeolian archipelago linking the mixing process to eruptive events.

Supplementary material

Table SM1: Complete analytical dataset containing all the analytical determinations performed on the experimental (877 analysis) and natural (92 analysis) samples. A total of five and three transects were analyzed for the experimental and the natural samples, respectively. The values of the calculated concentration variance (σ^2) for each chemical element in each transect are also reported.

Table SM2: Coefficients (C_1, C_0 and R) used to fit the decay of the concentration variance for the experimental samples and used to estimate the mixing-to-eruption timescales for the natural sample.

Figure

Figure 1

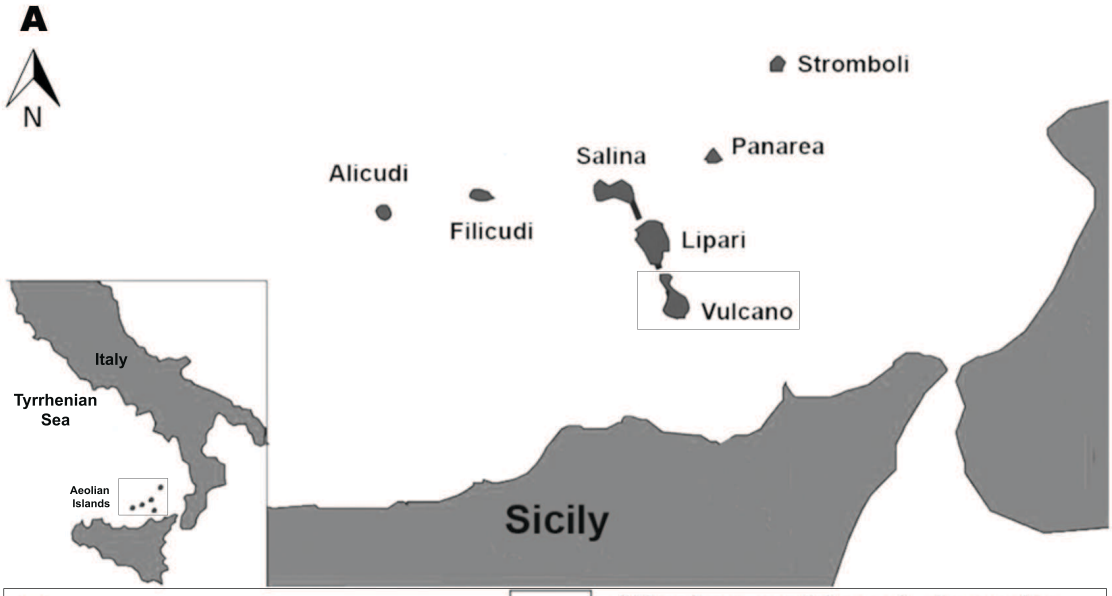

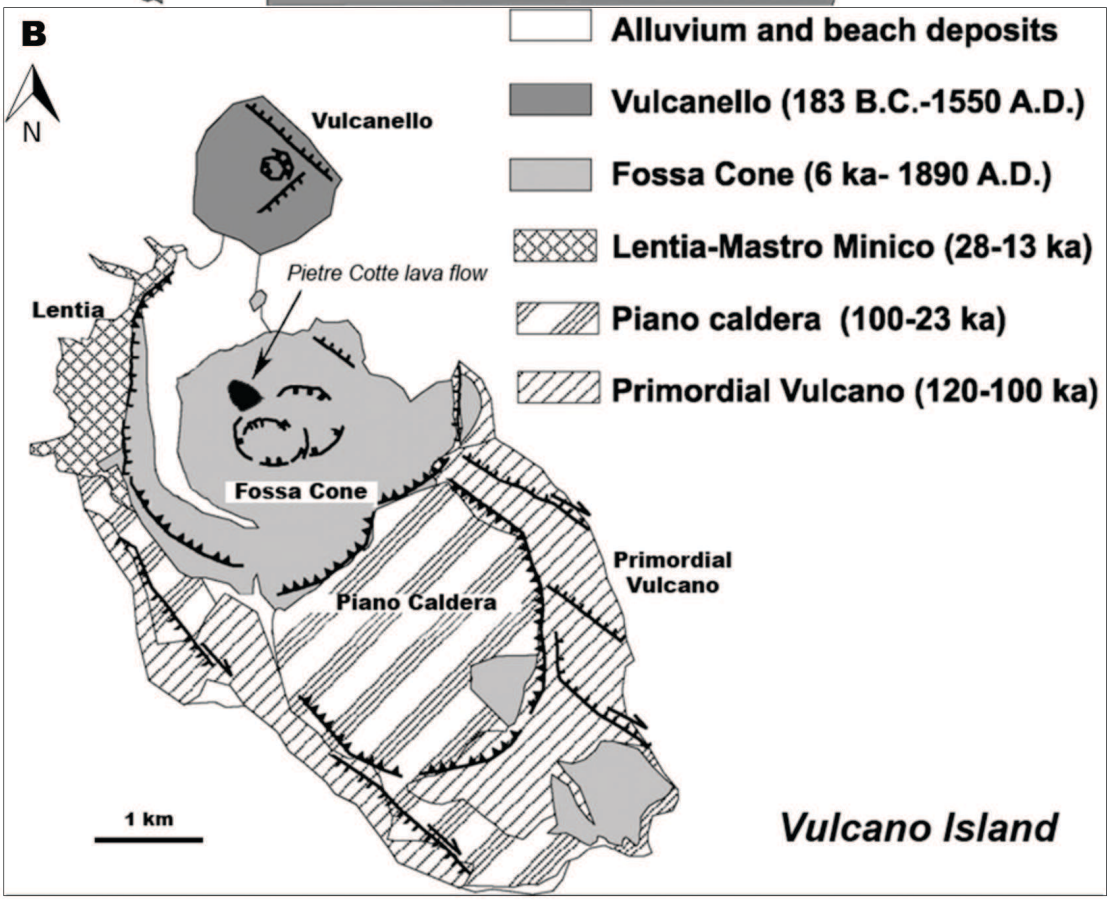

Figure

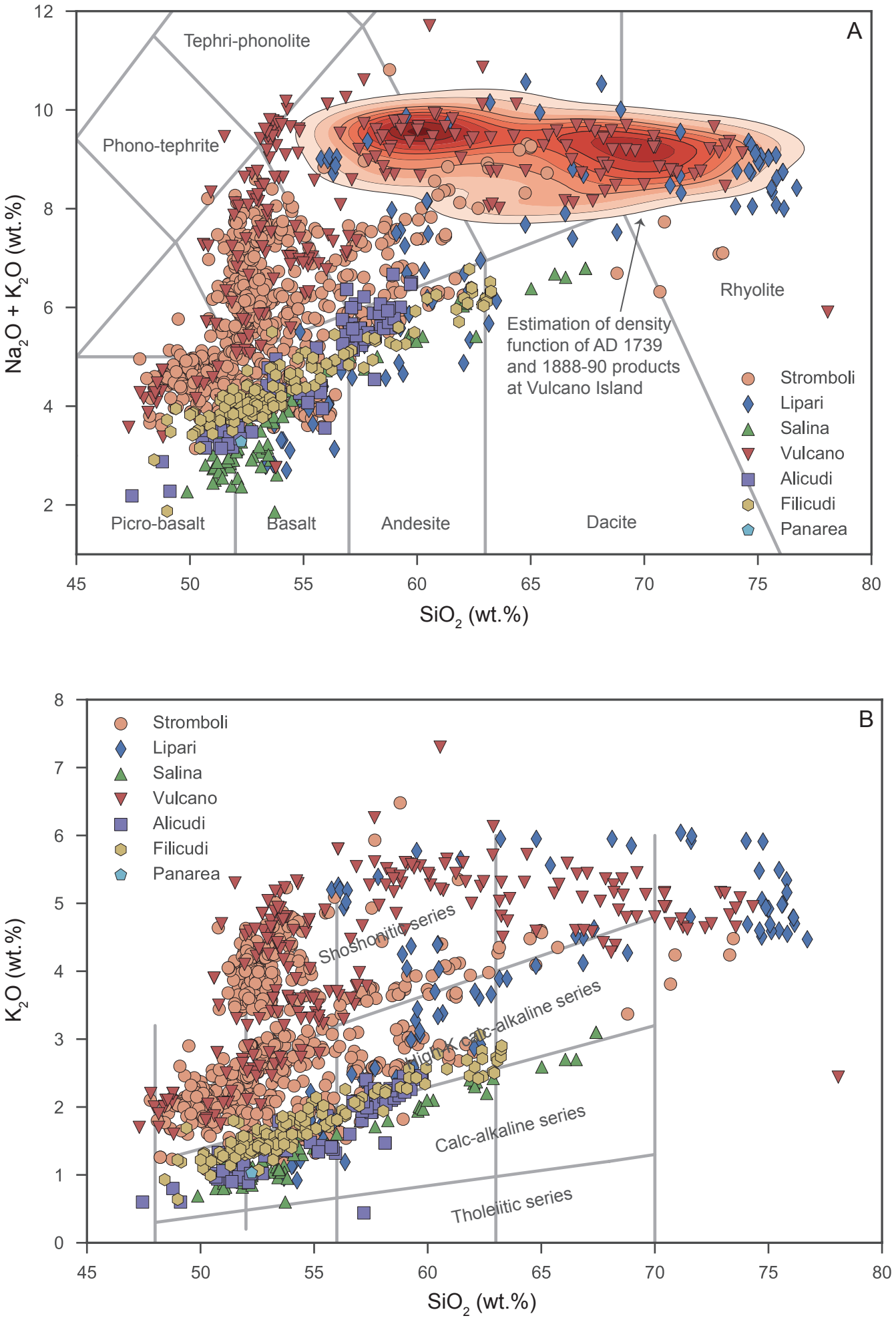

Figure 2

Figure

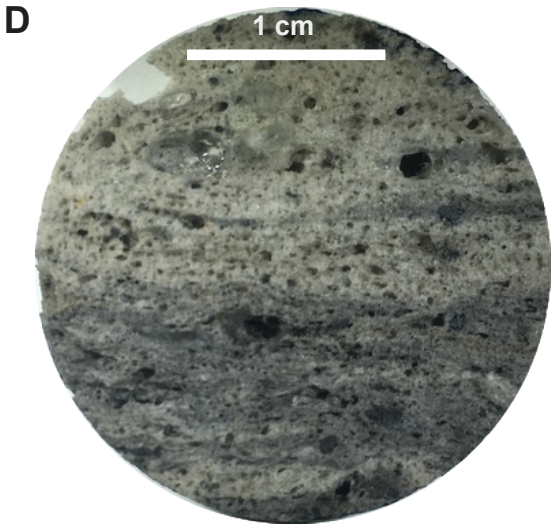

Figure 3

Figure

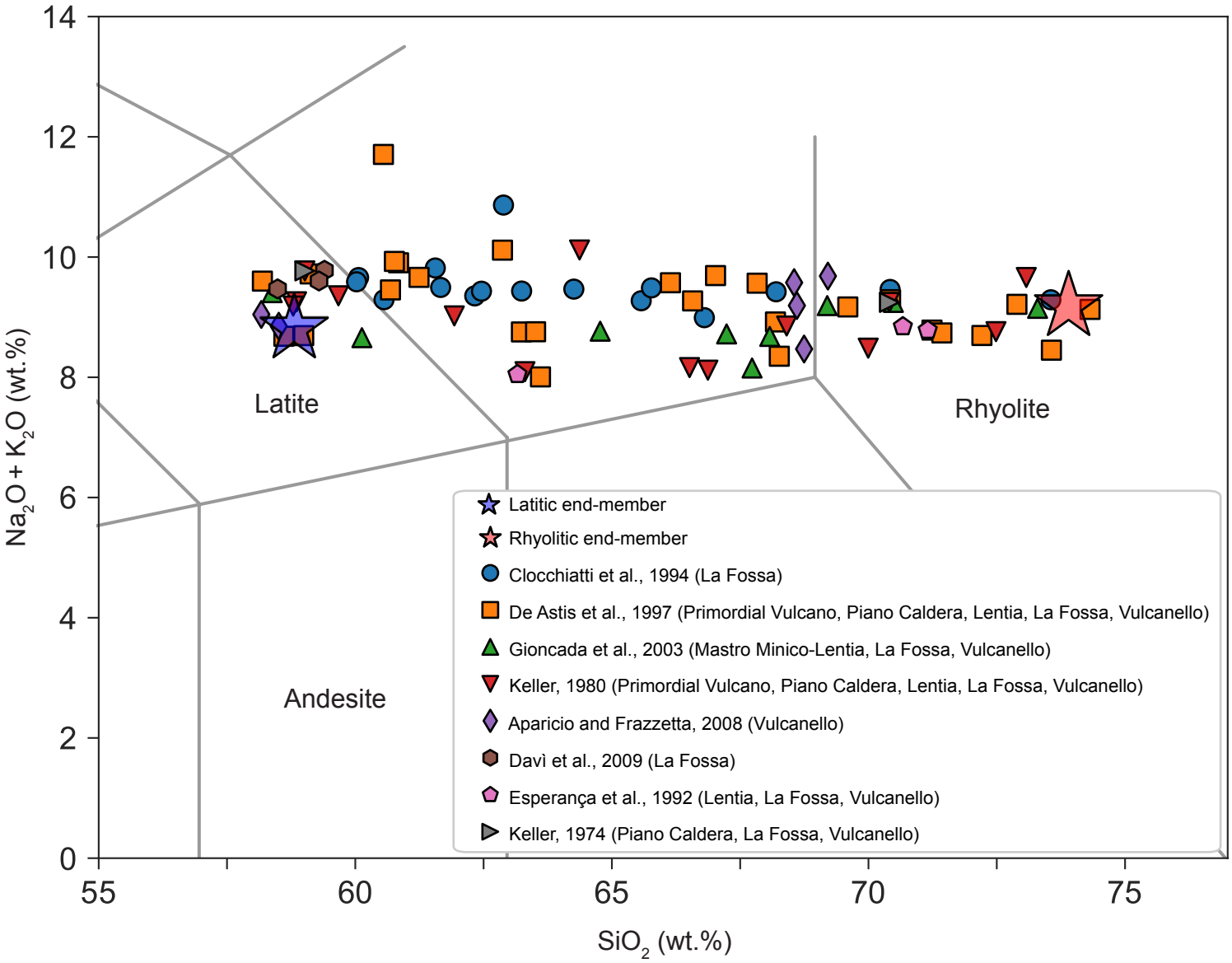

Figure 4

Figure

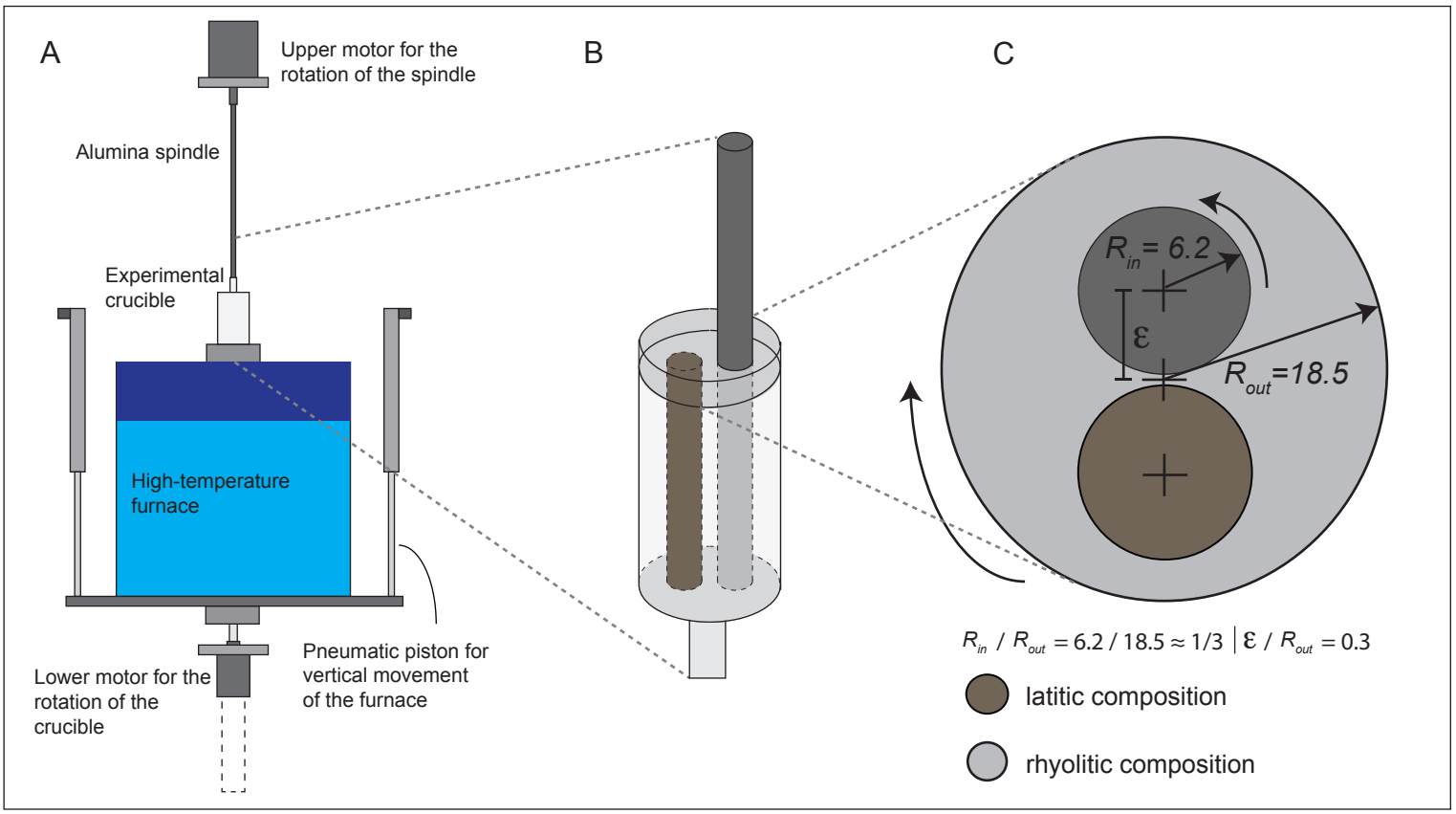

Figure 5

Figure

Figure 6

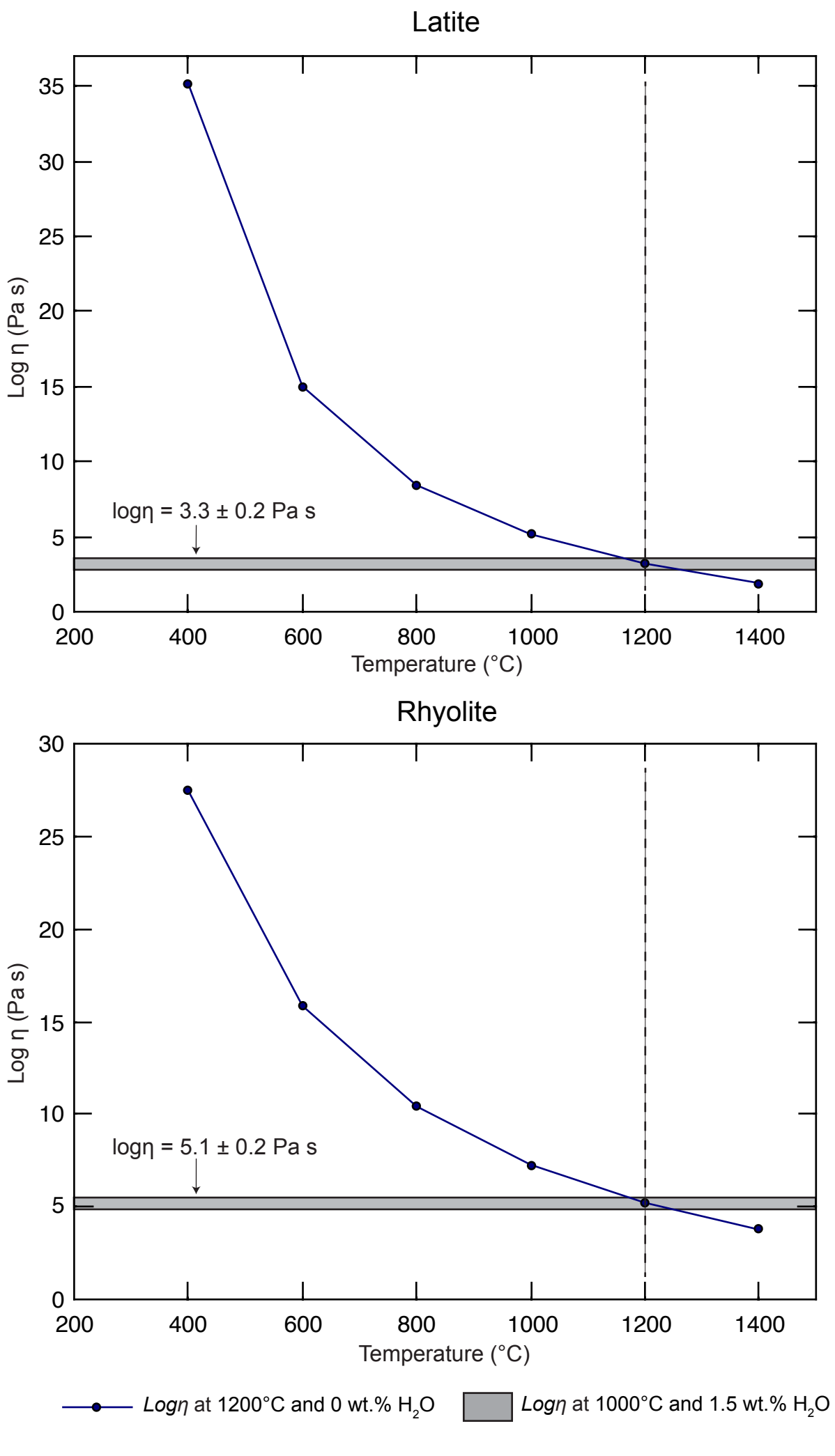

Figure

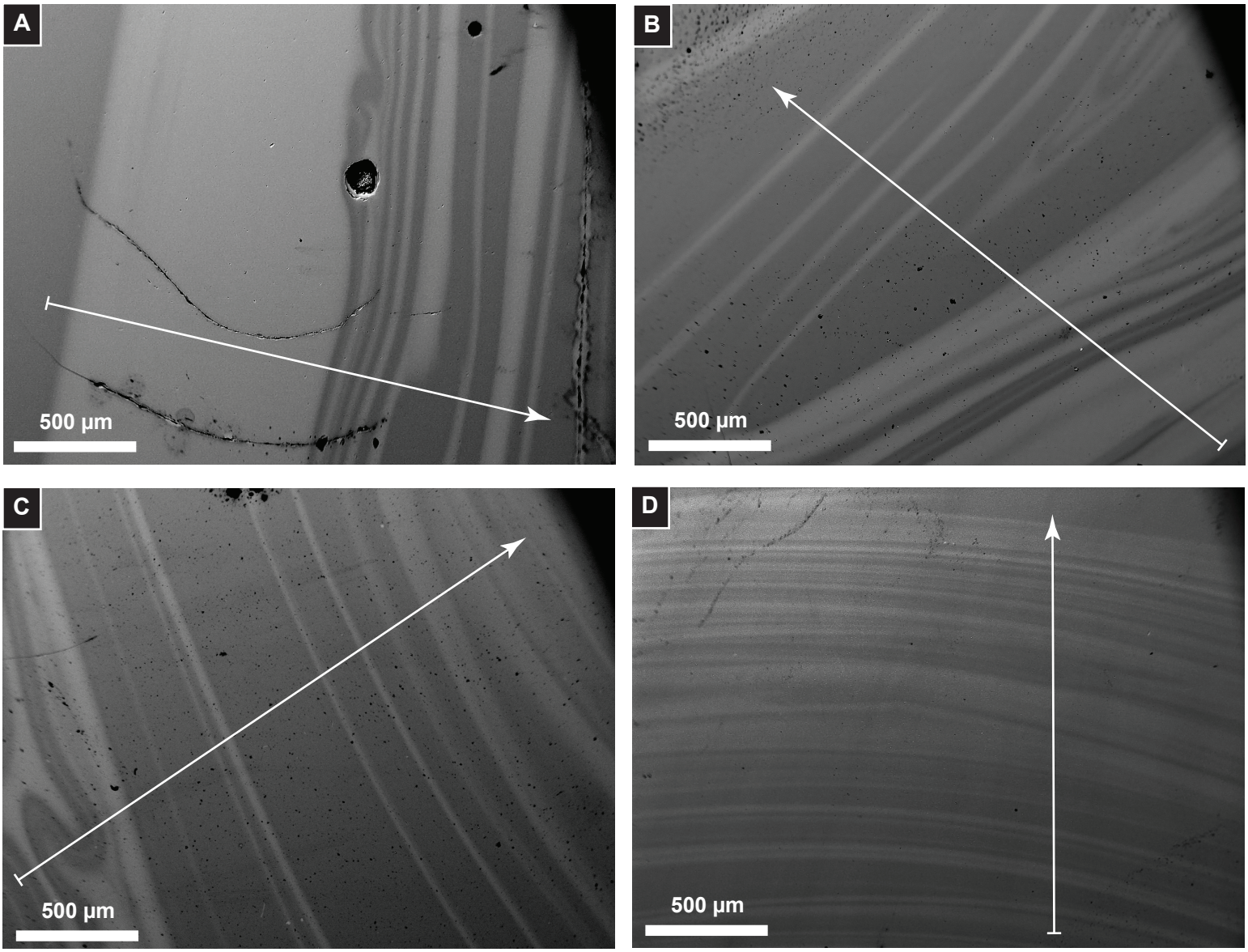

Figure 7

Figure

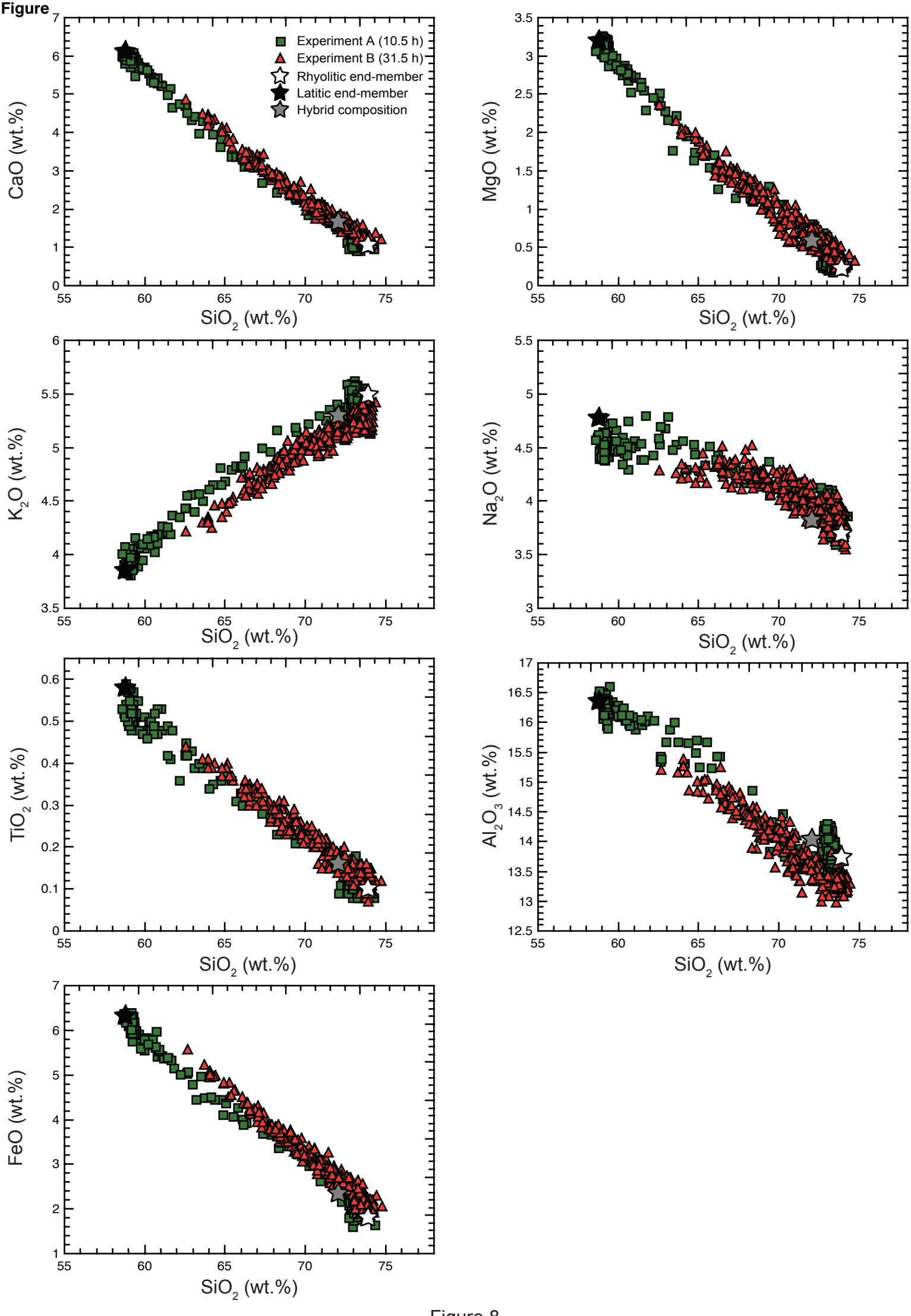

Figure 8

Figure

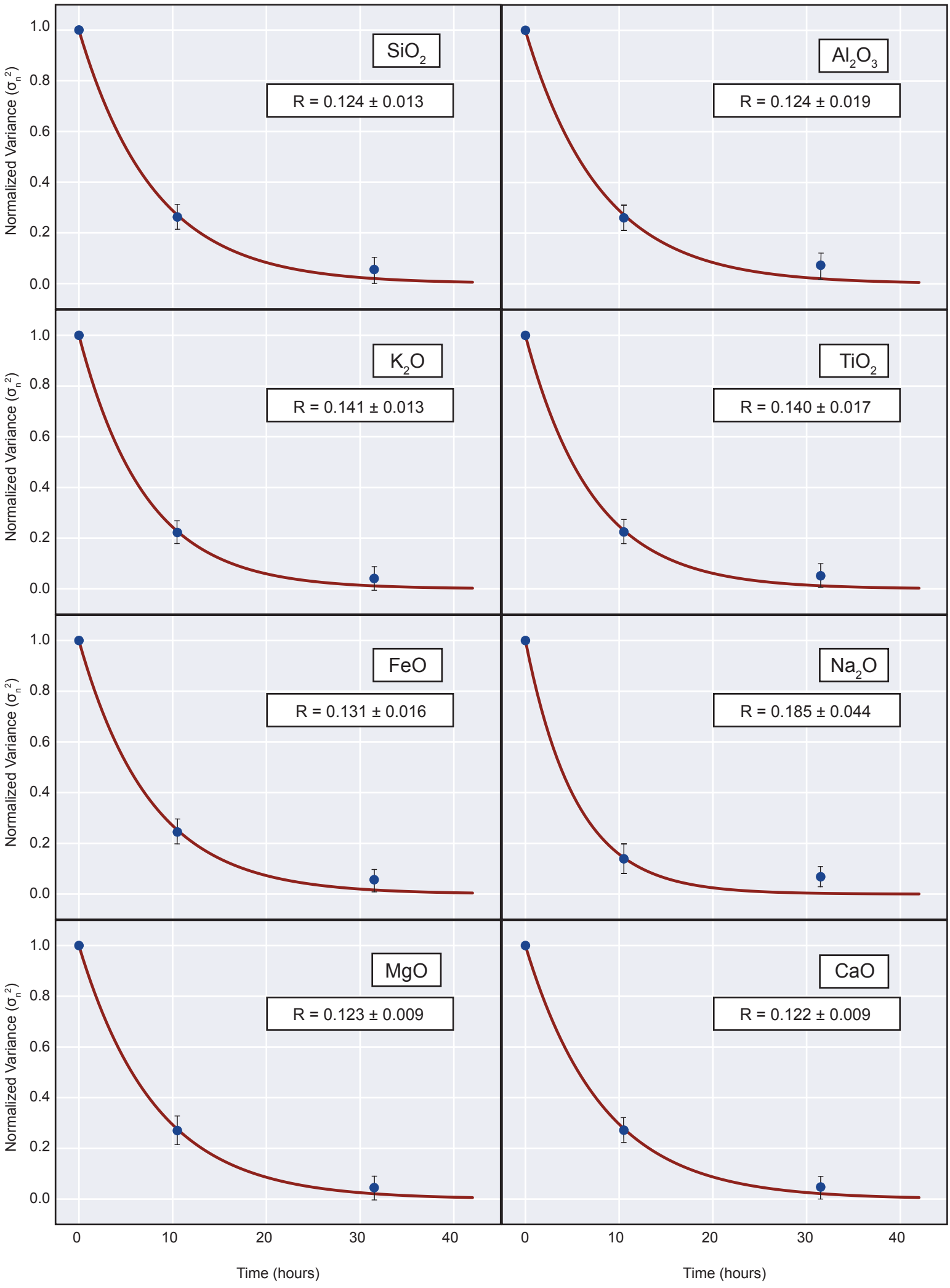

Figure 9

Figure

Figure 10

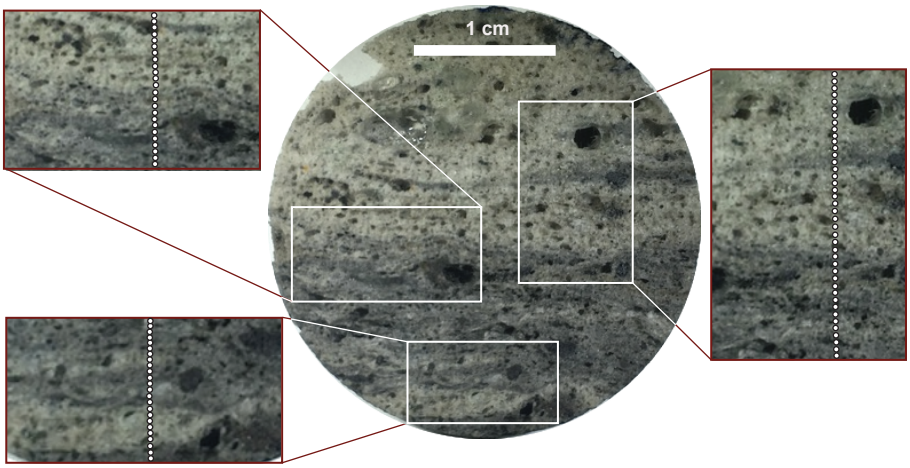

t = estimated mixing time

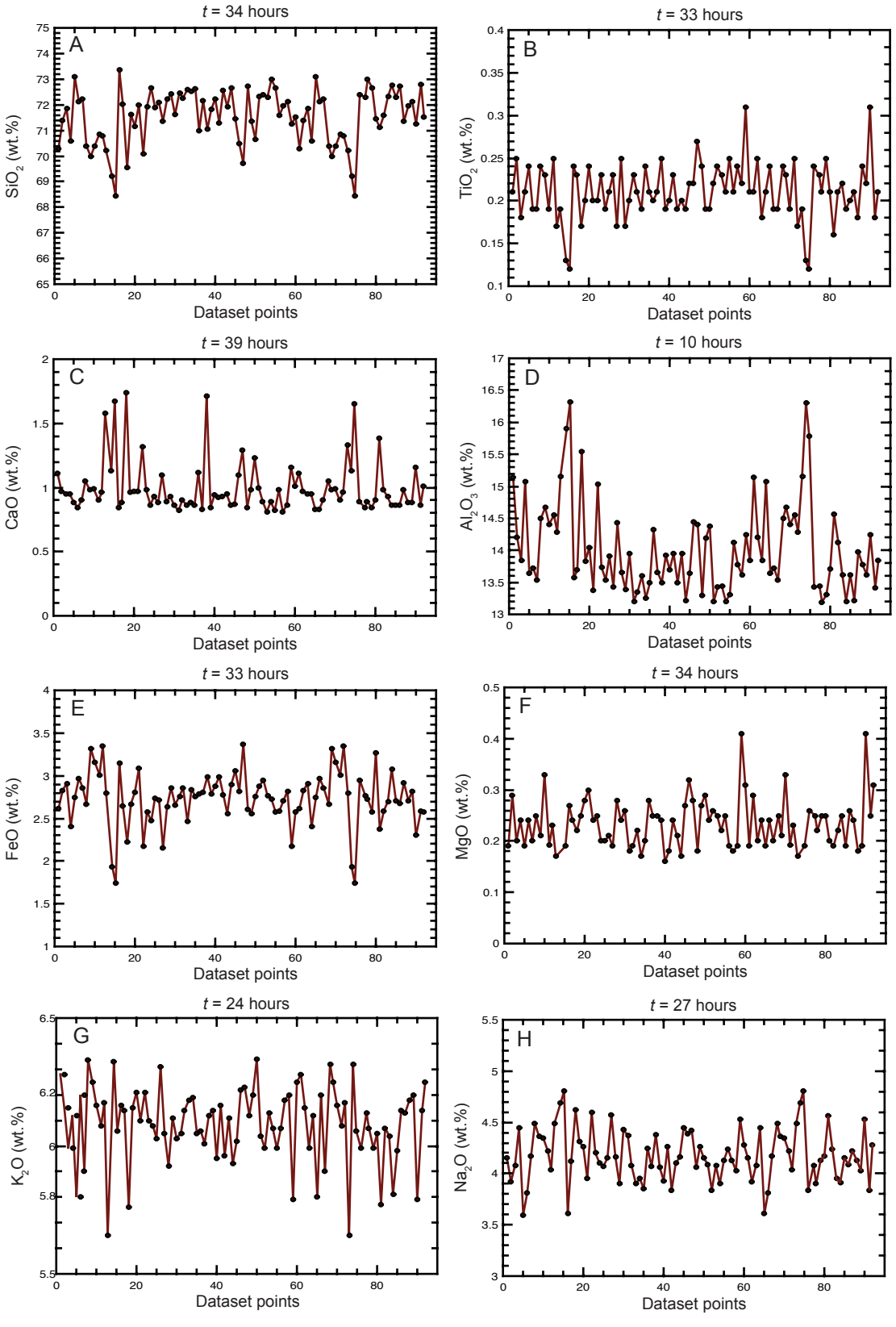

Figure

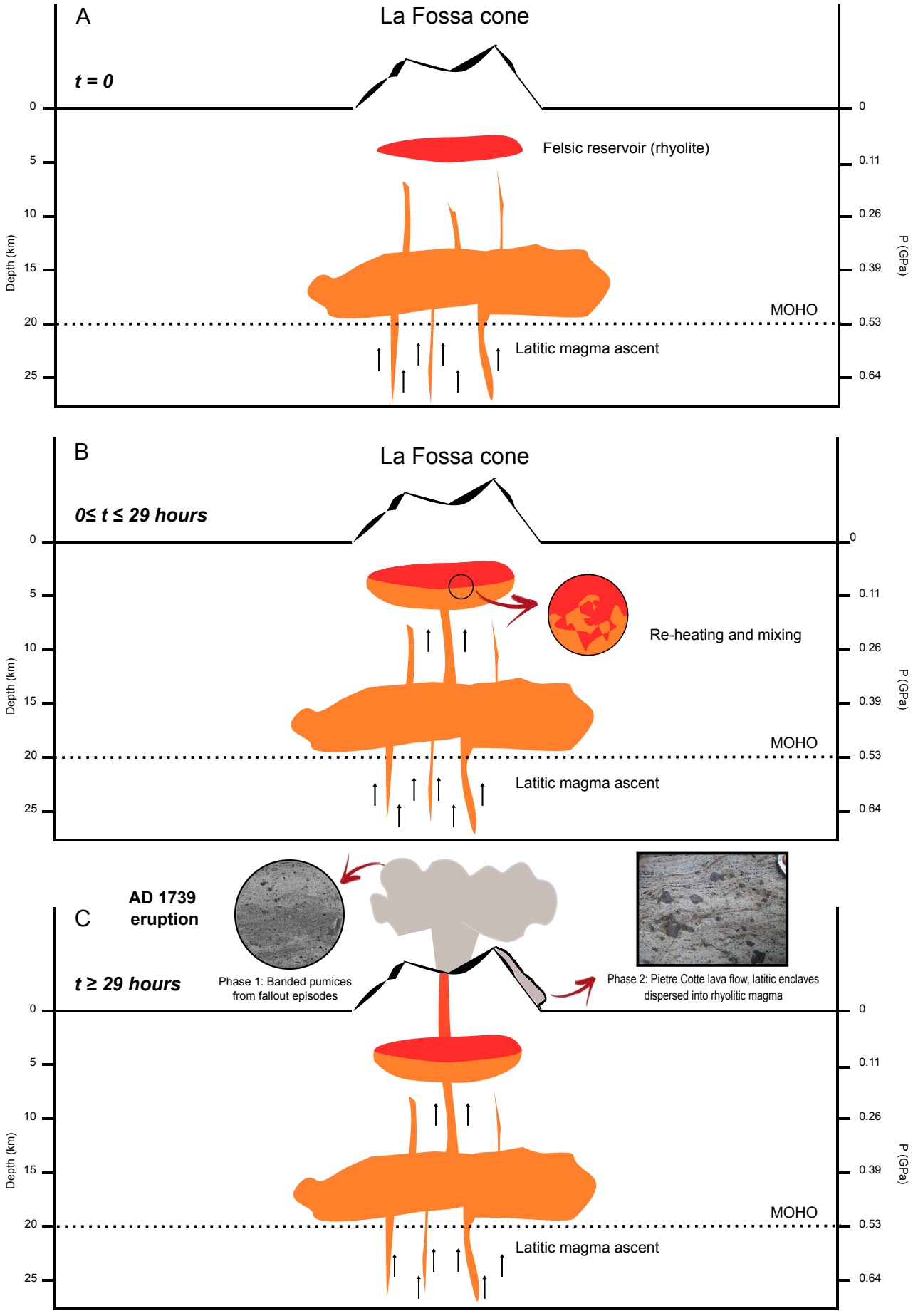

Figure 11

Table
Click here to download Table: Table 1 .docx

	Rhyolitic end-member (wt.%)	St. Dev.	Latitic end-member (wt.%)	St. Dev.
N=8				
SiO_2	73.90	0.2	58.81	0.4
Al_2O_3	13.73	0.3	16.36	0.2
K_2O	5.49	0.1	3.85	0.2
TiO_2	0.10	0.1	0.58	0.1
FeO_t	1.81	0.1	6.31	0.1
Na_2O	3.69	0.3	4.77	0.2
MgO	0.22	0.1	3.20	0.1
CaO	1.05	0.1	6.12	0.1
Total	100.00		100.00	
Density (g/cm^3)	2.35		2.54	
Viscosity (Pa s) @1200°C	1.66×10^5		1.62×10^3	

Table 1

Table
Click here to download Table: Table 2 .docx

Island	Eruptive event	Evidence of magma mixing	References
VULCANO	AD 1739 Pietre Cotte eruption	Latitic enclaves dispersed in a rhyolitic host magma	*Perugini et al. (2007)* *Piochi et al. (2009)* *Vetere et al. (2015)*
SALINA	Porri lava flow, age ca. 43 ka	Basaltic-andesitic enclaves dispersed in a dacitic host magma	*De Rosa et al. (1996)* *Ventura et al. (2006)*
	Upper Pollara eruption, age ca. 13 ka	Heterogeneous juvenile fragments (andesitic in composition) dispersed in a rhyolitic host magma	*Perugini et al. (2004)*
LIPARI	Monte Guardia eruption, age ca. 22 ka	Latitic enclaves (showing zoned plagioclase and clinopyroxene) dispersed in a rhyolitic host magma	*De Rosa et al. (2003)* *Gioncada et al. (2005)*
	Rocche Rosse lava flow, AD 1230 eruption	Latitic enclaves dispersed in a rhyolitic host magma	*Davì et al. (2009, 2010)*
STROMBOLI	1985-2000 and 2002-2003 activity products	Chemical zoning, resorptions and disequilibrium textures in clinopyroxene, olivine and plagioclase	*Landi et al. (2004, 2009)* *Armienti et al. (2007)*
	1985-1986, 1996 + Present-day activity products	Radiogenic isotope variations in clinopiroxene, olivine and plagioclase	*Francalanci et al. (2012)*
	Post Pizzo pyroclastic sequence and Present-day activity products	Chemical zoning in clinopyroxene and plagioclase	*Petrone et al. (2006, 2018)*

Table 2

Table

Click here to download Table: Table SM1 .xlsx

Dataset points	SiO_2	Al_2O_3	K_2O	TiO_2
				Profile
1	72.86	14.23	5.19	0.10
2	72.87	14.12	5.24	0.14
3	73.09	14.09	5.25	0.13
4	73.17	14.06	5.22	0.13
5	72.97	14.04	5.22	0.12
6	73.46	13.83	5.24	0.11
7	72.82	14.26	5.23	0.10
8	73.16	14.27	5.26	0.12
9	73.28	14.08	5.24	0.12
10	73.17	13.94	5.25	0.10
11	73.17	14.03	5.19	0.13
12	73.19	13.99	5.28	0.09
13	73.15	14.19	5.24	0.13
14	73.16	14.35	5.33	0.10
15	73.10	14.07	5.22	0.11
16	73.27	14.02	5.30	0.14
17	73.14	14.00	5.30	0.10
18	73.26	13.92	5.32	0.10
19	73.26	14.15	5.30	0.13
20	73.05	14.10	5.32	0.12
21	73.02	14.10	5.25	0.09
22	73.18	14.01	5.34	0.11
23	73.14	14.25	5.25	0.09
24	72.83	14.27	5.28	0.13
25	73.24	14.07	5.29	0.11
26	73.12	14.10	5.26	0.13
27	73.43	13.96	5.31	0.13
28	72.76	14.18	5.37	0.11
29	73.28	14.06	5.32	0.13
30	73.32	14.01	5.25	0.12
31	73.04	14.13	5.27	0.14
32	73.20	14.24	5.36	0.11
33	73.15	13.95	5.35	0.16
34	73.11	13.97	5.33	0.11
35	73.01	14.07	5.25	0.09
36	73.02	13.91	5.48	0.08
37	73.20	13.90	5.46	0.10
38	73.49	13.89	5.24	0.13
39	73.17	14.09	5.32	0.12
40	73.26	14.00	5.33	0.12
41	72.93	14.13	5.40	0.12
42	73.59	13.78	5.42	0.12
43	73.15	13.77	5.43	0.14
44	70.35	13.75	5.10	0.21

Table

Click here to download Table: Table SM2.docx

Oxide	**C_1**	**C_0**	**R**	***t (hours)***
SiO_2	0	1	0.124	34
Al_2O_3	0	1	0.124	10
K_2O	0	1	0.141	24
TiO_2	0	1	0.14	33
FeO	0	1	0.131	33
Na_2O	0	1	0.185	27
MgO	0	1	0.123	34
CaO	0	1	0.122	39
			averaged ***t***	**29**
			stand. dev.	**9**

Table SM2